photonics

MDPI

Review

Ultrafast Laser Pulses for Structuring Materials at Micro/Nano Scale: From Waveguides to Superhydrophobic Surfaces

Daniel S. Correa [1,*], Juliana M. P. Almeida [2], Gustavo F. B. Almeida [2], Marcos R. Cardoso [2], Leonardo De Boni [2] and Cleber R. Mendonça [2,*]

1 National Laboratory for Nanotechnology in Agribusiness (LNNA), Embrapa Instrumentação (CNPDIA), 13560-970 São Carlos, SP, Brazil

2 São Carlos Institute of Physics, University of São Paulo, PO Box 369, 13560-970 São Carlos, SP, Brazil; julianamara@ifsc.usp.br (J.M.P.A.); gustavo.foresto.almeida@gmail.com (G.F.B.A.); cardosomr@ifsc.usp.br (M.R.C.); deboni@ifsc.usp.br (L.D.B.)

* Correspondence: daniel.correa@embrapa.br (D.S.C.); crmendon@ifsc.usp.br (C.R.M.); Tel.: +55-16-21072800 (D.S.C.); +55-16-3373-8085 (C.R.M.)

Received: 6 December 2016; Accepted: 25 January 2017; Published: 31 January 2017

Abstract: The current demand for fabricating optical and photonic devices displaying high performance, using low-cost and time-saving methods, prompts femtosecond (fs)-laser processing as a promising methodology. High and low repetition femtosecond lasers enable surface and/or bulk modification of distinct materials, which can be used for applications ranging from optical waveguides to superhydrophobic surfaces. Herein, some fundamental aspects of fs-laser processing of materials, as well as the basics of their most common experimental apparatuses, are introduced. A survey of results on polymer fs-laser processing, resulting in 3D waveguides, electroluminescent structures and active hybrid-microstructures for luminescence or biological microenvironments is presented. Similarly, results of fs-laser processing on glasses, gold and silicon to produce waveguides containing metallic nanoparticles, analytical chemical sensors and surface with modified features, respectively, are also described. The complexity of fs-laser micromachining involves precise control of material properties, pushing ultrafast laser processing as an advanced technique for micro/nano devices.

Keywords: femtosecond laser; device fabrication; micromachining; optical glasses; doped polymer

1. Introduction: Fundaments of Femtosecond-Laser Material Processing

Advances in laser technology have produced lasers capable of emitting ultrashort pulses, with duration at the scale of femtoseconds. This characteristic have revolutionized laser material processing, a subject of research since the laser's first demonstration, which opened new possibilities for optical and photonic device development [1–3]. In femtosecond-laser micromachining, enough energy from the laser light is deposited onto the material to cause superficial or volumetric permanent change on the order of micro/nanometers. The specific features of the obtained microstructures depend on experimental parameters, such as wavelength, pulse energy, repetition rate, pulse duration, focusing objective numerical aperture and scan velocity. From a material science point of view, its optical and thermal properties are crucial to determining how matter will respond to intense light irradiation.

Once material modification at ultrashort pulse regime is related to aspects fundamentally different from those that rule the micromachining process with longer pulses, an understanding of light-matter interactions is of foremost relevance to understanding material processing. One of the main reasons for these differences lies in the fact that at an ultrashort pulse regime the laser energy deposition occurs within the pulse duration, i.e. before any relaxation or thermalization processes have been initiated.

Material electronic configuration is responsible for the energy absorption and primary heating, while the atomic lattice remains nearly unaltered. Heat transfer from highly excited electrons to ions and further thermalization followed by diffusion begins long after the pulse has left the material [4]. In this scenario of heavy non-equilibrium conditions, the decoupling between electronic and lattice systems allows their temperatures to be treated independently according to the well-known Two-Temperature Model [5–7].

Another main reason why femtosecond-laser micromachining provided new avenues for material processing lies in absorption, which is governed by nonlinear processes due to the extremely high peak intensities delivered by ultrashort pulses. Although the promotion of nonlinear effects deeply influences the microfabrication of absorptive materials, the most striking phenomenon is the nonlinear absorption in transparent materials. Linear absorption effect occurs when an electron is promoted from the ground to the excited state by one-photon absorption. Clearly, the energy $h\nu$ of this single photon has to be enough to overcome the energy gap E_g between those states, otherwise absorption does not take place. In nonlinear absorption, a group of photons with insufficient individual energy to perform the linear absorption acts together to produce material excitation and, eventually, ionization. There are two regimes involved in the nonlinear ionization: the photo-induced and avalanche mechanisms. The first one suggests that promotion of electrons to the conduction band is due to the laser field, specifically by either multiphoton ionization or tunneling. Multiphoton ionization is described by the simultaneous absorption of n photons by a single electron, which is consequently excited from the valence to the conduction band. Here, the energy combined of all involved photons has to exceed the bandgap energy in such a way that ionization can occur, $nh\nu \geq E_g$. Photoionization can also be achieved by a tunneling process facilitated by the distortion of the atomic potential caused by the laser electric field. Both previously described ionization processes are, in fact, part of the same phenomenon modeled by Keldysh [8] in 1965, differentiating themselves by laser intensity level and wavelength.

Avalanche ionization is the result of a repetitive sequence of events, which includes free carrier absorption and impact ionization. At first, an electron excited to the conduction band absorbs subsequent photons raising its energy up to a level that exceeds the minimum of conduction band energy. Later, this highly energetic electron collides with an electron occupying the top of the valence band and, through this impact ionization, both electrons end up in the lowest level of the conduction band [9,10]. The process repeats for the excited electrons, promoting new electrons from the valence band to the conduction band. This mechanism continues to occur during the presence of the intense laser light and leads to an exponential growth in the population of the excited electrons. A requirement for the avalanche ionization is the presence of seed electrons in the conduction band so that the process can start. In the case of femtosecond-laser pulses, these seeds mostly originate from the photoionization mechanisms mentioned before, but defect states close to the conduction band may facilitate the seed electron creation. The light absorption is strongly enhanced by the plasma formed as the electron density in the conduction band increases drastically and its frequency matches the laser frequency. At this critical point, plasma becomes nearly opaque to the incident wavelength and absorbs a great amount of energy that later evolves to energy relaxation and material modification.

In general, femtosecond-laser micromachining is classified into two major types of material modification: ablation and damage. Ablation is the process that usually occurs at the surface of the target material, in a timescale on the order of hundreds of nanoseconds, resulting in material removal. The rule of nonlinear absorption in femtosecond (fs)-laser ablation has been recently investigated [11]. The non-equilibrium condition brings extreme complexity to the physical mechanisms involved during ablation. Among the most accepted ones are the Coulomb explosion [12], material ejection, and evaporation [13]. One of the great achievements of the ultrashort pulse ablation is the capability of producing a minimal heat-affected zone surrounding the laser spot region. It is because significant deposited energy is taken away with the early stages of the material removal and less heat is diffused into the lattice.

The process of bulk damage takes place in transparent material. Once nonlinear absorption is highly dependent on laser intensity, only at the focus there is enough intensity to produce ionization leading to optical breakdown. Such a characteristic enables the microfabrication of three-dimensional structures into the material bulk, without modifying regions outside the focal volume of the laser beam, inscribing, for example, waveguides [14] and photonic crystals [15]. Novel applications of fs-laser micromachining in micro-supercapitors [16], microlenses [17] and biosensors [18] have also been proposed and demonstrated.

There are two main structural changes observed in bulk damage experiments. By using laser energy level close to the material threshold, changes in the refractive index [3,19] can be produced, which is attributed to material melting and subsequent fast resolidification [20–22]. This variation in the refractive index can be positive or negative, according to an increase or decrease in the material density that is accompanied by the rapid cooling [23]. In the opposite energy level range, well above the material threshold, the production of empty voids [24–26] due to microexplosions that lead to a hollow or less dense regions in the focal volume (where material has been expanded) is observed [27,28]. When using an intermediate energy level, the induced modification can result in an alternated composition variation, denominated nanograting, which leads to a birefringence in the microstructured region [29]. Other review papers in this field, presenting not only applications but also fundamental aspects of fs-laser micromachining, have been recently published [30,31].

As previously mentioned, produced damage depends on laser and material features, as well as on the experimental conditions, thus, different results can be observed in fs-laser micromachining. Optical and thermal properties of materials are crucial to determine how the material responds to intense light irradiation. Experimental parameters, such as pulse duration, pulse energy and numerical aperture of the focusing lens define the light intensity, which along with laser wavelength define the induced optical nonlinearity. Among the experimental parameters, the laser repetition rate plays an important role in thermal effects caused by fs-pulses. Because laser energy is first deposited into the electronic system and because it is only after the highly excited electrons are thermalized with the lattice that heat diffusion occurs, heat is carried away from the focal volume in a time scale of the order of 1 μs. Therefore, the interval between adjacent pulses directly influences the microfabrication process, which can be carried out in two distinct regimes. When using fs-oscillators that emit pulses with energy on the order of nJ at a repetition rate of MHz, the micromachining exhibits a cumulative behavior, since pulses are separated by a time much shorter than the characteristic time for heat diffusion. In this scenario, the energy deposited from a pulse cannot be dissipated before the next pulse arrives at the same place. Therefore, after sequential pulses, the accumulated heat inside and outside of the focal volume reaches critical level, leading to structural change. The focal volume acts as a heat source of micrometer dimensions emanating heat for as long as the laser exposure time. In contrast, amplified laser systems deliver pulses with energy on the order of μJ and with repetition rate in the range of kHz. In this way, the micromachining takes place in a repetitive regime, since pulses are separated by millisecond, which is significantly larger than the heat diffusion time. As a consequence, the material returns to equilibrium at room temperature before the next pulse strikes it again. This means that produced microstructures are restricted to the focal volume, presenting very little collateral damage in its vicinity [32].

In the next sections, we present some details about how the fs-laser can be used to modify distinct materials at surface/bulk, aiming particularly at applications in optical waveguides, photonic structures and superhydrophobic surfaces.

2. Experimental Aspects of fs-Laser Material Processing

Although there are several fs-laser-based techniques employed for obtaining materials at micro- and submicro scales, one of the most common approaches relies on focusing the fs-laser into the sample, either in its volume or on its surface, depending on the desired goal. From the experimental viewpoint, the laser light is focused into the sample using microscope objectives with different numerical apertures

(NAs), as shown in Figure 1. Alternatively, depending on the desired size of the features, lenses with larger focal distances can be used. Hence, as illustrated in Figure 1, a specific pattern is produced by either *x*-*y* sweeping the laser beam on the sample, which is kept fixed, with the aid of galvanometric mirrors (Figure 1a), or by using a three-dimensional (*x*-*y*-*z*) stage to translate the sample in respect to the fixed focusing lens (Figure 1b). In the first case (Figure 1a), the movement in the *z*-axis is achieved by an additional translation stage. The choice of which approach should be used depends on experimental details, such as processing time and area, laser repetition rate, etc. The movement of the sample or laser beam deflection is computer controlled, which defines not only the processing pattern on the sample but also the material processing speed, which is directly related to the number of pulses per laser spot for a given laser repetition rate. In order to visualize the material processing in real time, usually a CCD camera is coupled to the experimental setup.

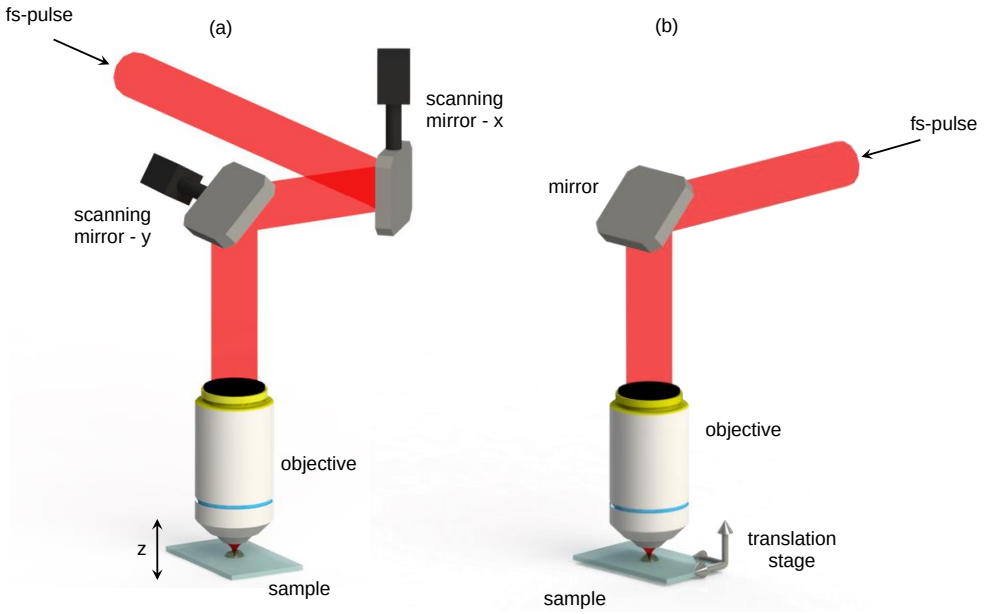

Figure 1. Schematic diagram of the experimental setup for femtosecond (fs)-laser processing of materials using (**a**) laser beam scanning mirror for beam deflection and (**b**) *x*-*y*-*z* translation stage for the sample.

When fs-pulses are focused onto a material, the irradiance reached at the focal volume can be high enough to induce optical nonlinearities, i.e., for intense and tightly focused laser pulses, the corresponding electric field can achieve magnitudes comparable to the ones that bind the electrons in atoms or molecules, leading to a nonlinear optical phenomenon (e.g. multi-photon absorption). Because the multi-photon absorption is localized into the focal volume, the resulting structural changes [33,34], photoreduction [35,36], degradation [37] and ablation [38], will also be confined to the vicinity of the focus, which can be exploited to advance materials processing.

The light irradiance required to produce changes in materials is determined by three experimental parameters: pulse energy (E), pulse duration (τ) and numerical aperture (NA) of the focusing objective. Usually, the highest value of E and the shortest pulse duration are specified by the laser system being used. When τ and NA are set, the nonlinear absorption will be exclusively dependent of E. In this circumstance, the threshold energy is defined as the smallest value of E for which changes in the material occur. When E is increased above the threshold, the sample-affected zone is typically larger than the focal volume, whereas for E, close to the threshold, changes are localized to the focal region. The feature size achieved by laser processing is essentially determined by NA, which defines the focal width and depth. The geometry of the structured region is also influenced by NA; while spherical

features are obtained for high NA (typically higher than 0.6), asymmetric structures are observed when small NAs are used.

Fs-laser processing can be achieved in several types of materials, including polymers and glasses, using energy per pulse on the order of nanojoules, which can be accomplished through fs-laser oscillators that operate with repetition rate in the scale of MHz. When material processing is carried out using such oscillators, the heat diffusion time is longer than the interval between consecutive pulses, which confers a cumulative character onto the process [39,40]. On the other hand, when amplified femtosecond sources are used, which generally operate with a kHz repetition rate, the nature of the micromachining process is repetitive [39]. Ti:sapphire laser oscillators, operating at a wavelength of approximately 800 nm and repetition rate of MHz, are still the most used laser sources for fs-laser processing of materials, although other sources based on fiber femtosecond oscillators have gained significant attention. The quality, resolution and properties of the fs-laser-processed samples are usually evaluated by microscopy techniques, such as optical, atomic force and scanning electron microscopy, as well as by standard spectroscopic tools, such as UV-Vis, Fluorescence and Raman.

Other experimental setups that include interference and diffraction processes have also been developed, allowing the fabrication of complex microstructures without the need of scanning the laser beam or translating the sample. For example, arbitrary shapes were microfabricated by using Spatial Light Modulators, which are used to apply amplitude/phase masks to the beam prior to focusing [41,42]. Diffractive optical elements (DOE), such as diffractive beam splitters play an important role in the multifocal micromachining [43] and in the fabrication of periodic microstructures [44–46]. The basic idea behind the use of DOE is to produce multiple laser beams that are later focused at different angles, producing an interference pattern. Such modulation in the laser intensity is then transferred to the structure micromachined in the sample.

Besides the micromachining setups mentioned previously, multiphoton polymerization (MPP) can also be used to fabricate micro- and nanometer-sized three-dimensional structures. In this approach, a photoinitiator molecule, when excited via multiphoton absorption, triggers a polymerization reaction, allowing the fabrication of microstructures [47]. The spatial resolution achieved in such microstructures can be drastically improved by incorporating the concept of stimulated emission depletion (STED) [48], which can reduce the resolution to tens of nanometers [49]. Many applications could benefit from the combination STED-MPP, particularly the fabrication of photonic crystals operating in the visible range of the spectrum that require periodic structures on the order of few hundreds of nanometers [50].

3. Fs-Laser Processing of Distinct Materials

3.1. Optical Waveguides in Polymers

Fs-laser microfabrication can be used for producing optical devices in several types of polymers since they can present high optical transparency, good mechanical properties and feasibility for laser processing. For instance, poly(methylmethacrylate) (PMMA) is a low-cost polymer that has high optical transparency in the ultraviolet (UV) and infrared (IR) spectral regions and also presents a refractive index similar to standard glass optical fibers. Such features make it quite suitable for designing optical devices, including micro-optical lenses and waveguides. In addition, other organic or inorganic compounds (such as chromophores) can be added to PMMA aiming at modifying its linear and nonlinear optical properties.

For instance, the fabrication of tubular waveguides using a Ti:saphire oscillator fs-laser has been reported in PMMA doped with Disperse RED 13 (DR13), which is an organic chromophore [51]. The fabricated waveguides were characterized by optical microscopy, as the one displayed in Figure 2 (top view). The pulse energy employed during the fabrication process was of 42 nJ, and yielded small black dots on its center, which were attributed to the thermal damage at the zone surrounding the focus. The authors attributed the damaged zone to a carbonized portion of the material originated during the fs-laser fabrication, due to the very high light intensities employed for the fabrication.

Figure 3a displays a top view image (by transmission optical microscopy) of an isolated waveguide [51]. Using a HeNe laser beam, the authors coupled light to the waveguides, whose near-field intensity distribution is shown in Figure 3b. No light was guided through the waveguides' central region due to absorption, although on the annular region (of higher refractive index), light was reasonably guided with azimuthal symmetry. The total loss estimated for this waveguide was 0.8 dB/mm.

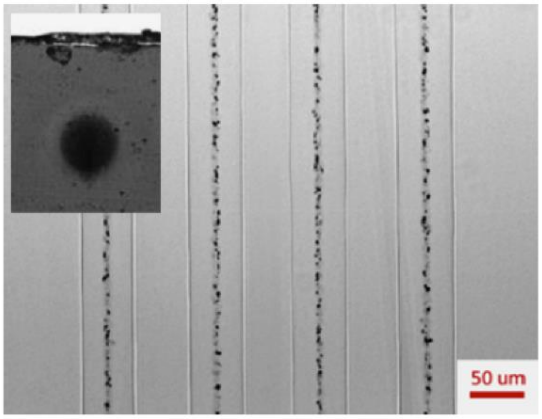

Figure 2. Optical microscopy image of waveguides produced with an energy of 42 nJ and scanning speed of 100 μm/s. The inset shows a transverse image of a typical waveguide. Reprinted with permission from [51]. Copyright (2014) Elsevier.

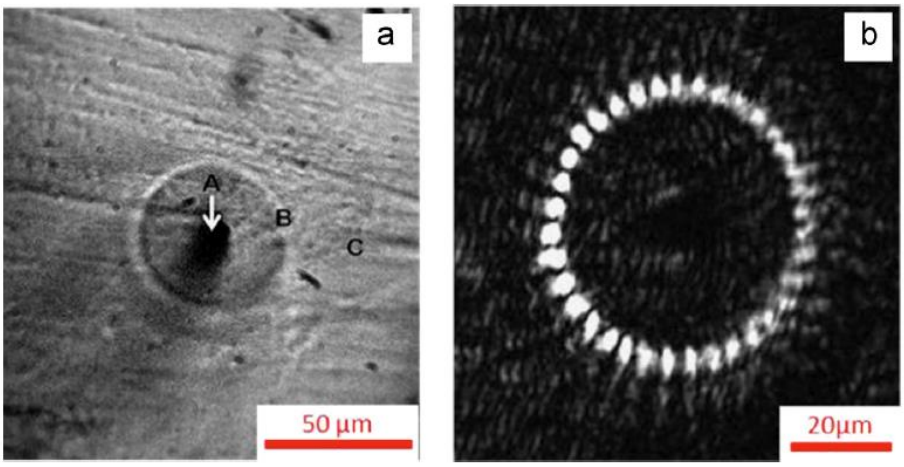

Figure 3. (**a**) Transmission optical microscopy image and (**b**) near-field intensity distribution of the output waveguide at 632.8 nm. [51]. Copyright (2014) Elsevier.

The domain of experimental parameters along with the understanding of local refractive index change has enabled the fabrication of waveguides in PMMA with a virtually symmetric fundamental mode and a propagation loss of 0.5 dB/cm [52]. The guiding area is a consequence of the beam refocusing, resulting in a secondary modification region where polymer damage or negative refractive index changes are avoided. In order to improve the waveguide performance in PMMA, a phase-retrieval algorithm has also been proposed to identify the internal structure and modifications caused by laser pulses [53].

3.2. Fluorescent Polymeric Structures

Poly[2-methoxy-5-(2-ethlyhexyloxy)1,4-phenylenevinylene] (MEH-PPV) is a flexible, easy-to-process [54] conjugated polymer with outstanding electrical and optical properties,

which are interesting for photonic applications [55]. Taking advantage of these features, fs-laser micromachining of MEH-PPV films has been carried out by researchers, as reported by [56]. In that study, the authors produced 14 µm thick MEH-PPV films by casting a solution of this polymer on a Teflon recipient over a glass substrate. In order to create microstructures on the film, femtosecond-laser micromachining was carried out using a Ti:sapphire laser that delivered 50 fs pulses, centered at 800 nm, operating at a repetition rate of 5.2 MHz. The microstructured lines produced in the film were measured via optical microscopy as a function of the pulse energy (0.2 to 2 nJ) for scanning speeds of 20, 50, 75 µm/s, yielding lines with widths from 0.6 to 10µm. Two distinct processes for the fs-laser processing were observed: (i) for lower energy regimes, only morphological changes were observed, while (ii) for higher energy regimes, polymer removal was achieved. Atomic Force Microscopy (AFM) images of the irradiated lines revealed that, for energy below the ablation threshold, a protuberance was formed as a result of mechanical stress on the film due to heating, melting and subsequent solidification. On the other hand, when laser pulses with energy above 1.0 nJ were employed, material removal on the film was observed. Figure 4 shows the sample topography obtained with both energy regimes. Also, from AFM images, the average surface roughness of specific areas was twice as large at regions close to the micromachined line, probably because of debris expelled from the ablation process. Furthermore, it was observed that the average roughness increased as a function of the pulse energy, since the material removal becomes more efficient.

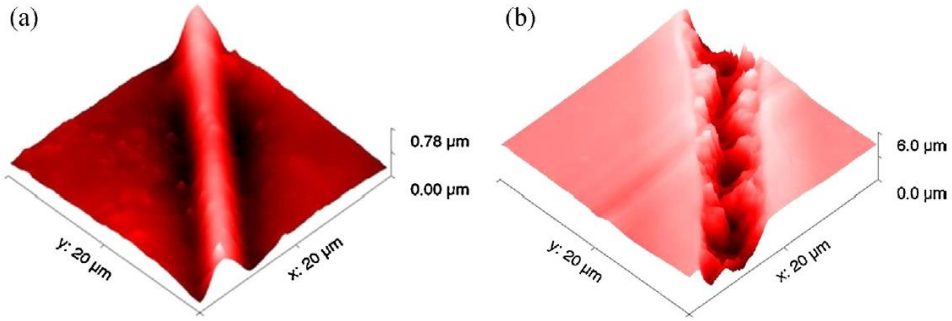

Figure 4. Sample topography from Atomic Force Microscopy (AFM) of structures induced on MEH-PPV film by using laser pulse energy of 0.6 nJ (**a**) and 1.1 nJ (**b**) at scanning speed of 25 µm/s. Reprinted with permission from [56]. Copyright (2014) Elsevier.

The influence of fs-laser micromachining on the MEH-PPV films' optical properties was evaluated by the absorption spectrum of areas containing microfabricated lines, separated by 4 µm and fabricated with distinct pulse energy at constant speed of 50 µm/s. It was observed that the band centered at 500 nm, which is characteristic of MEH-PPV absorption, decreased as a function of the pulse energy due to a photobleaching process induced on the sample. Since this polymer is transparent at 800 nm (excitation wavelength employed) but exhibits a strong two-photon absorption cross-section [57], such bleaching was attributed to a multi-photon photo-oxidation [58]. In addition, the authors also showed the functionality of the microstructure by fabricating an electroluminescent device based on a thin film (*ca.* 300 nm) of MEH-PPV spin-coated on Indium Tin Oxide (ITO) substrate, which was partially laser ablated and presented electroluminescence under applied voltage.

Femtosecond laser has also been applied to produce active microstructures via two-photon absorption polymerization (2PP). This technique enables the fabrication of neat and doped polymeric microstructures with high definition and virtually no shape constraints, finding application in optical, electrical and biological devices [59–64]. For instance, [65] the fabrication of three-dimensional microstructures based on triacrylate monomers and ZnO nanowires using a fs-laser experimental setup delivering pulse energies of 0.5 nJ has been reported. The fabricated composite microstructures containing 1% of ZnO dispersed in the polymeric matrix displayed good structural integrity, as can be seen in the scanning electron microscopy (SEM) images displayed in Figure 5.

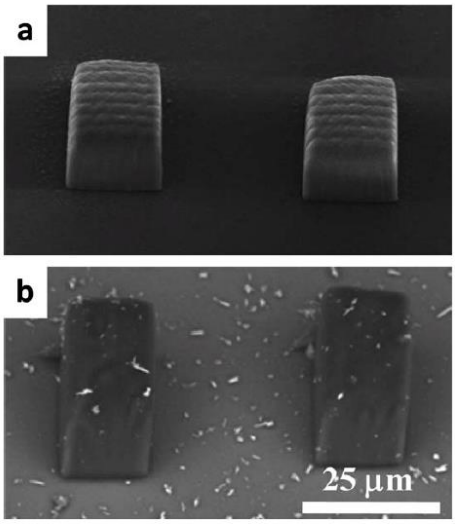

Figure 5. SEM images of two-photon polymerized ZnO nanowires/polymer composite microstructures containing 0.5 (**a**) and 1.0 (**b**) wt % of ZnO nanowires. Reprinted with permission from [65]. Copyright (2014) Wiley Online Library.

Such microstructures are interesting for designing optical devices due to their intense fluorescence. For this purpose, the authors employed a cw He-Cd laser operating at 325 nm with an average power of 12 mW to beam on the sample. Figure 6 reveals a broad and intense emission of the ZnO nanowires/polymer composite microstructure, with the emission peak centered at approximately 570 nm due to oxygen vacancy defects in Zn. The inset of Figure 6 shows the fluorescence (top view) image of such a ZnO nanowires/polymer composite microstructure containing 5 wt % of ZnO nanowires, which was excited using a cw laser at 350 nm.

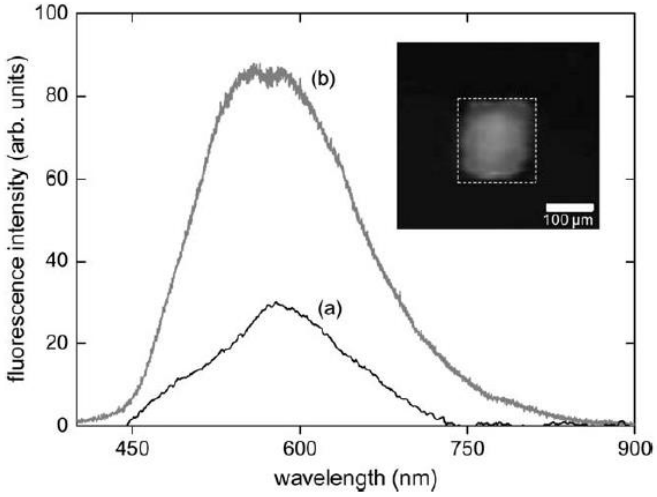

Figure 6. Emission spectra of the ZnO nanowires/polymer composite microstructure containing 5 wt % of ZnO nanowires (**a**) and for the ZnO nanowire powder (**b**). The inset shows the fluorescence image (top view) of a cubic microstructure containing ZnO. Reprinted with permission from [65]. Copyright (2014) Wiley Online Library.

Two-photon polymerization was also employed by Otuka et al. [59] to fabricate concentric cylindrical polymeric shells using a multi-step fabrication process. The outer cylindrical shell was composed by undoped acrylic resin, while the inner one was composed of the same acrylic resin doped with Rhodamine B. Figure 7a displays a scanning electron microscopy image of such structure

(top view), while (b) and (c) display optical and fluorescence microscopy images respectively. In (b) it is possible to observe parts of the cylindrical structure; the center with air, the inner cylindrical shell doped with Rhodamine B and the outermost with net polymer. This cylindrical microstructure, when excited with light at 450 nm from a LED source, exhibited a strong fluorescence that was confined to the inner cylindrical shell containing Rhodamine, while only a small scattering was observed in the outermost cylinder (Rhodamine-free region). Such polymeric structures are interesting for fabricating optical microcavities with distinct dopants.

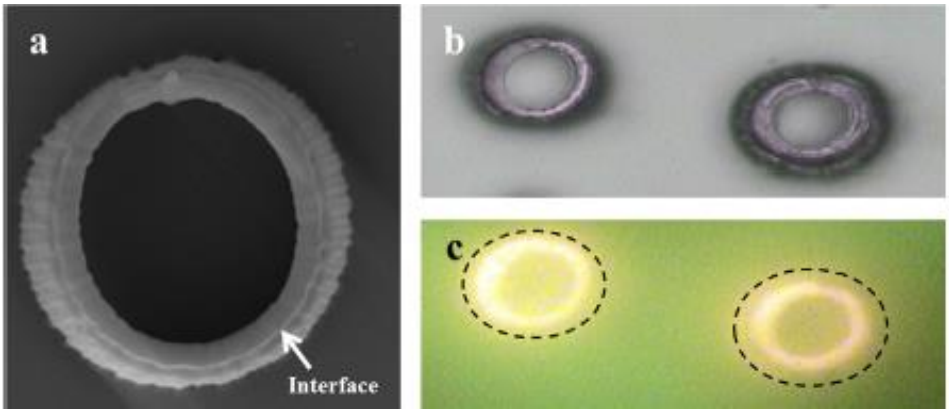

Figure 7. (**a**) SEM and (**b**) optical image (top view) of the cylindrical microstructures (the external diameter of the cylinder is 30 μm with a thickness of 5 μm), displaying the interface between the cylindrical shells. (**c**) Fluorescence image of the microstructure upon excitation with an LED centered at 450 nm. The contour of the undoped region is represented by the dotted line. Reprinted with permission from [59]. Copyright (2014), Materials Research.

Optical storage devices (OSDs) can also be achieved via 2PP. For instance, highly dense OSDs were fabricated by de Miguel et al. by spatially selecting the fluorescence functionalization of doped microstructures. The fluorescence images obtained from the structures revealed that the proposed method was qualified for producing precise pixels as small as 0.24 μm^2 by adjusting the pulse energy, which enhanced the dye fluorescence due to an induced diaggregation effect caused by thermal effects [66].

3.3. Superhydrophobic Polymeric Surfaces

Laser processing has also been employed for producing surfaces exhibiting dual-scale roughness, aiming at applications from microfluidics to self-cleaning devices [67–70]. For instance, Furstner et al. [67] investigated the wetting and self-cleaning properties of three types of superhydrophobic surfaces. They observed that surfaces containing two levels of roughness presented self-cleaning features under artificial rain. Jiang et al [71] fabricated superhydrophobic surfaces based on polyorganosiloxane using a sol-gel and heat treatment process followed by coating with a nanosilica (SiO_2) sol and organosiloxane 1,1,1,3,5,5,5-heptamethyl-3-[2-(trimethoxysilyl)ethyl]-trisiloxane (β-HPEOs). The wettability of polyorganosiloxane films changed from hydrophobic to superhydrophobic, presenting water contact angles from 144.5 ± 0.7° to 156.7 ± 1.1°, while the hysteresis angle decreased from 6.5 ± 0.6° to 2.5 ± 0.6°. Wang et al. [68] applied superhydrophobic sol-gel on canvas to promote self-cleaning ability. A solar cell device with nanoscale morphology was demonstrated by Zhu et al. [69], which presented higher power efficiency than a flat film device and enabled self-cleaning due its topological features. Guan et al. [72] used microinjection compression molding with dual-layer molds to replicate a bio-inspired 3D topography. The micropattern was coated with submicro silica particles that confer dual-scale topography on the mold. Furthermore, by modifying surface topological features, one should expect to observe changes in the aerodynamic

and hydrodynamic, hydrophobic and hydrophilic properties, optical absorption, as well as van der Walls force interaction, as observed in geckos' feet [73].

Since the wettability of surfaces depends on their topology and chemical nature [74–78], strategies combining both aspects have been developed to obtain superhydrophobic materials [75,79–83]. As a natural example of a superhydrophobic surface, the lotus leaf has inspired the fabrication of synthetic superhydrophobic surfaces. One way to study the wettability properties of surfaces is by measuring the contact angle with water, in which higher angles indicate higher hydrophobicity. Therefore, the large water contact angle (CA) of the lotus leaf, on the order of 160°, is attributed to the combined effect of its covering wax and surface structure [84]. In fact, the lotus leaf presents a hierarchical surface structure that is composed of a dual-scale roughening at the micro- and nanoscale [84,85].

The process of mimicking the lotus leaf pattern on an artificial surface is a complex subject, because it involves precise control over surface microstructuring, while keeping the already obtained nanostructure on the surface. In order to reproduce the lotus leaf's superhydrophobic effect on synthetic surfaces, a combination of chemical modification and patterning of the sample has been employed [86–88]. Several methods, from extruding of polymers [89] to femtosecond-laser microfabrication [74] have been proposed to design superhydrophobic surfaces [67,74,75,79,81–83,88,90,91].

A hierarchical structuring process that combines stamping (nanoscale) and laser micromachining (microscale) has been performed by Cardoso et al. in order to create highly hydrophobic surfaces [92]. This approach combined advantages of both methods, such as the flexibility for the nanoscale fabrication, provided by stamping, and the selectivity of fs-laser micromachining. Furthermore, both methods can be applied to a large range of materials. For example, the surface pattern of ZnO nanowires was transferred to polydimethylsiloxane (PDMS) by stamping, which resulted in a nanostructured PDMS surface. Subsequently, this film was micromachined by femtosecond-laser pulses in order to create a periodic microstructured surface, using 150 fs pulses from a Ti:sapphire-amplified laser, operating at 780 nm with a repetition rate of 1 kHz and pulse energy of about 0.5 μJ [92]. The fabricated samples presented good uniformity, thanks to the consistency of stamping and laser micromachining. The resulting surfaces were composed of pillars with squared cross-sections, with periodicities of 10, 20, 30, and 40 μm. Figure 8 shows AFM micrographs of the hierarchical surface (micro- and nanostructures) produced on the PDMS sample. The depths of the grooves produced by micromachining, determined by AFM, are on the order of 4 μm.

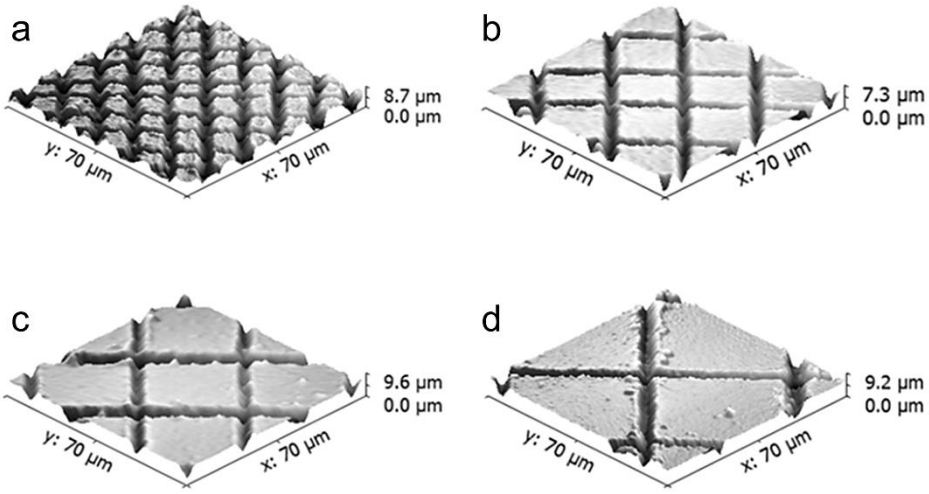

Figure 8. Atomic force microscopy (AFM) images of nano/microstructured polydimethylsiloxane (PDMS) films with periodicities of 10 μm (**a**), 20 μm (**b**), 30 μm (**c**) and 40 μm (**d**). Reprinted with permission from [92], Copyright (2015), Wiley Online Library.

The hierarchical surface structuration, achieved by stamping and subsequent laser micromachining, presented an increase of nearly 49° (from 121° for the flat surface to 170° for the structured one), while the contact angle hysteresis (CAH) was determined as 3° [92].

3.4. Superhydrophobic Metallic Surfaces

The irradiation of solids with linearly polarized Ti:sapphire femtosecond-laser pulses under normal incidence can result in laser-induced periodic surface structures (LIPSS). For metals or semiconductors, LIPSS has been observed with a period close to or slightly smaller than the irradiation wavelength and an orientation perpendicular to the laser beam polarization. The generation of the LIPSS is due to an interference of the incident laser beam with the surface electromagnetic wave generated at the rough surface, which might include the excitation of surface plasmon polaritons [93]. Similarly to fs-laser processing of polymers, femtosecond-laser pulses have also been used to make silicon surface hydrophobic. Baldacchini and co-workers used a train of 100 fs-laser pulses from a Ti:sapphire laser system focused at normal incidence on the surface of *n*-doped Si (100) wafers aiming to produce superhydrophobic surfaces [74]. They obtained different surface morphologies depending on laser fluence. The features of the surface topology for a range of fluence from 2.2 to 9.0 kJ/m^2 changed from laser-induced periodic surface structures to a coarsened surface to an array of cone-shaped spikes. All these surfaces, after laser micromachining, were treated with air plasma and terminated with fluorosilane to decrease the surface energy. The latter procedure allowed them to study the hydrophobic effect of roughness produced by laser structuring. The authors analyzed the effects of surface modification with different laser fluence upon the static and dynamic wetting properties. They found a superhydrophobic behavior for all laser micromachined samples with water contact angle of 160° and less than 3° contact angle hysteresis. They also measured contact angle for hexadecane on the microstructured silicon surfaces and observed that the microstructuring changed the contact angle from a wetting value of 79° on flat silicon to a nonwetting value between 105° and 129° on the laser-microstructured surface. Hexadecane exhibited a contact angle hysteresis between 22° to 33°, in contrast to water. For this work, the authors concluded that wetting properties of these surfaces followed the Cassie-Baxter model [94].

Zorba et al. [95] have achieved a similar change in the wetting properties of silicon by femtosecond-laser structuring. They used femtosecond laser to simultaneously create micro- and nano-patterns in silicon surfaces, whose wetting properties were investigated without any coating deposition. By increasing the fs-laser fluence from 0.17 to 1.8 J/cm^2, they achieved an enhancement of the water contact angle from 66° to more than 130°. One important contribution of that investigation was to show the possibility to use the femtosecond laser to fabricate a gradient of wettability on a silicon surface, which resulted in a spontaneous motion of water droplets. They have structured a series of successive regions with a number of laser fluences, resulting in different morphologies, consequently inducing a wettability gradient [95].

Kietzig et al. [96] have irradiated different metallic alloys with 150 fs-laser pulses from an amplified Ti:sapphire laser system that delivers pulses centered at 800 nm with a repetition rate of 1 kHz. A rough structure containing dual scale was created on the alloy surface immediately after laser irradiation. Using different laser fluences (0.78, 2.83 and 5.16 J/cm^2), distinct structures were obtained, as presented in the SEM images in Figure 9. In this figure, it is possible to see the polished surface and the regular protuberances after the laser process. It is clearly observed that surface roughness increased with laser fluence. Moreover, a dual-scale roughness is observed in the SEM images. For all fluences and materials, a periodic ripple structure (submicro scale) was observed on the disordered protuberances (micro scale). Wetting properties of the micromachined metal alloys were determined by contact angle measurements. Immediately after laser micromachining, samples presented superhydrophilic behavior, with water spreading out on the surface. Nevertheless, an increase on the contact angle was observed over time. The changes in wettability were attributed to the presence of carbon and its compounds on the laser-irradiated surfaces [96].

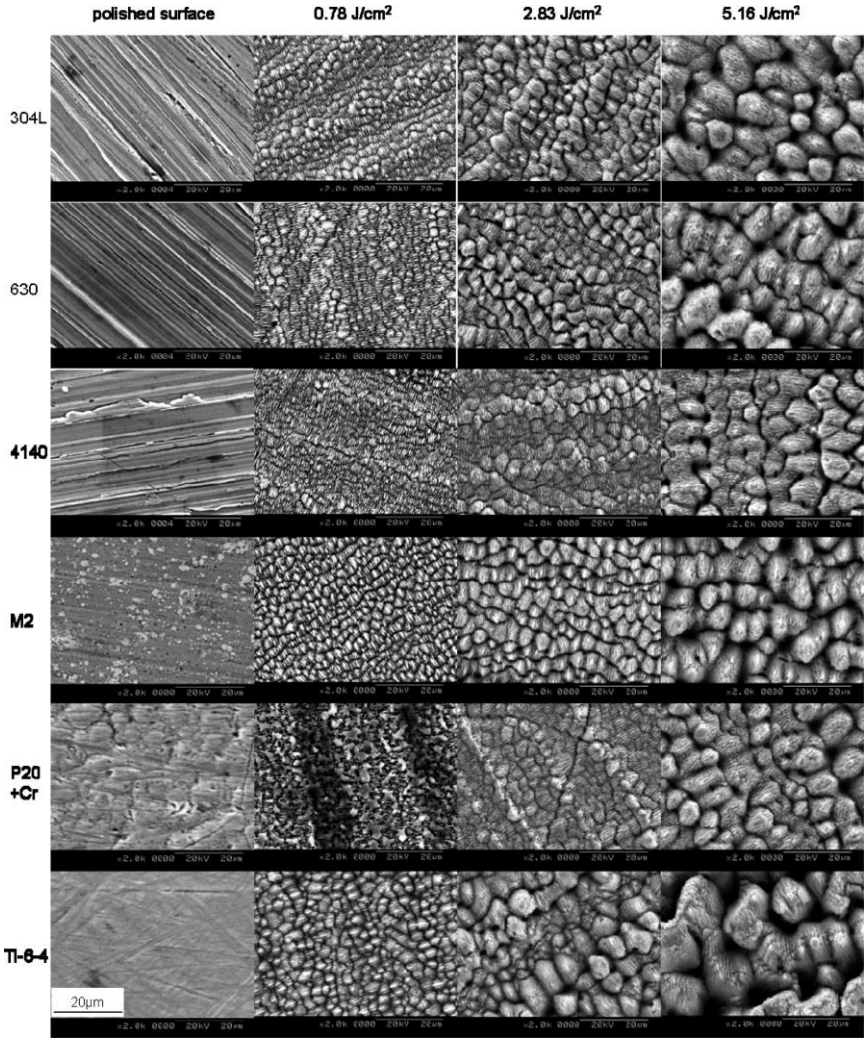

Figure 9. SEM images of polished and laser-structured surfaces with fluences 0.78, 2.83 and 5.16 J/cm^2. Reprinted with permission from A. Kietzig et al. 2009, Copyright (2009), ACS publications.

Similarly, Wu et al. [91] used femtosecond-laser pulses to structure stainless steel and subsequently cover the surface with silane agent to obtain superhydrophobicity. The authors observed the formation of 0.5 µm LIPSS [93] using laser fluences between 0.08 and 0.2 J/cm^2. Ripples, with periodicity of about 3.5 µm, started to appear with laser fluence of 0.24 J/cm^2, presenting smaller LIPSS structures with periods of approximately 0.35 µm. By increasing the laser fluence, periodic ripples and cone-shaped spikes at the micro scale were created. The base of the conical spikes presented an asymmetric feature, with the short axis of the base parallel to the direction of the laser polarization. In addition, the height of the spikes and distance between them increased with the laser fluence. With femtosecond-laser micromachining and subsequent silanization, stainless steel became superhydrophobic with the maximum contact angle with water of 166.3°. More recently, Li et al. [97] demonstrated the fabrication of rough hierarchical structures on Ti plates using femtosecond-laser pulses and achieved superhydrophilicity. After silanization, the previous structured Ti surfaces were converted to a superhydrophobic one displaying contact angle with water of 163.7°.

3.5. Optical Waveguides

3.5.1. Optical Waveguides in Glasses

Among inorganic materials, glasses have been one of the main targets for fs-laser processing. Such interest is based on the ability of causing permanent changes in the glass bulk, which can be used to provide active or passive functions to optical devices. The interaction of ultrashort laser pulses with the network results in nonlinear optical effects responsible for the local modification of glass properties. Usually, glasses used for fs-laser micromachining are transparent to the laser wavelength employed, but multiphoton absorption can occur, promoting electronic transitions from valence to the conduction band and/or new electronic configurations. This is the starting point for further nonlinear optical phenomena, such as tunnel, impact and avalanche ionizations, that lead to microscopic modification in glasses [39,98].

Alteration of the refractive index of glasses by fs-pulses stands out compared to other induced effects because the modified glass can act as optical waveguides, according to the illustration in Figure 10, which shows top and cross-section views of waveguides in a boron-based glass, as well as the light guided at 632.8 nm [99]. The first report on the fabrication of waveguides within the glass bulk revealed an increase in the refractive index ranging from 0.01–0.035 depending on the irradiation in pure and Ge-doped silica glass [1]. The same achievement was demonstrated for borosilicate, chalcogenide and fluoride glasses, in which structures with lower increase in the refractive index, on the order of 10^{-3}, were able to guide light at 800 nm, supporting propagations of mono- and multimodes [19]. These pioneer works gave rise to a large number of investigations about the physical processes behind the fabrication of waveguides in glass by fs-laser. It has been proposed that the formation of microplasma induces structural changes in the focal volume due to a non-elastic thermomechanical stress, affecting the local density [100]. Furthermore, the temperature may achieve values above the glass transition, resulting in melting and rapid quenching, which also changes the density and consequently the refractive index [1]. More recently, it has been demonstrated that the ultra-densification of porous glass using fs-laser may lead to refractive index change on the order of approximately 0.1 [101].

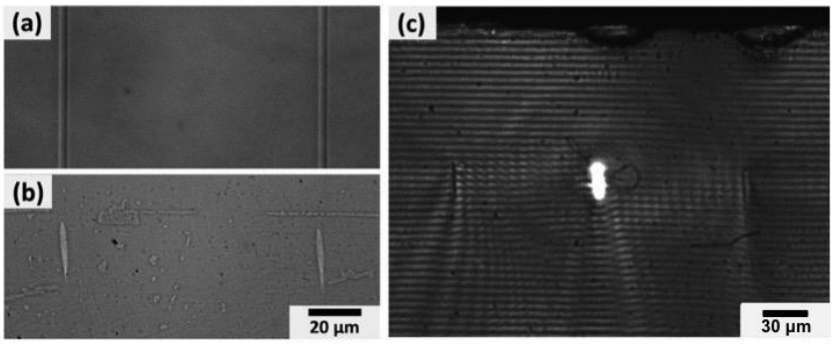

Figure 10. Images of waveguides produced in boron-based glass by femtosecond-laser pulses. Top (**a**) and cross-section view (**b**) of two parallel waveguides are illustrated along with the near-field output profile of the light guided at 632.8 nm (**c**). Reprinted with permission [99]. Copyright (2015), Elsevier.

The experimental parameters have a fundamental role over the fabrication process and waveguide features, in which the laser repetition rate directly affects the temperature at the irradiated region, whereas the average power, scan direction and numerical aperture of the objective lens mainly influence the waveguide size and shape [39]. Concerning the waveguide cross-section, elliptical or cylindrical structures are obtained when the sample is translated transversally or longitudinally to the laser beam, respectively [1]. This observation persists since the first developed waveguide and it is related to

the beam intensity profile at the focus. This is the region where nonlinear interactions take place; thus the confocal parameter ($b = 2\pi w_0^2/\lambda$) defines the waveguide cross-section when the sample is moved transversally to the beam propagation direction. On the other hand, when the translation is performed longitudinally to the beam propagation, the waveguide assumes the shape of the beam diameter, $2w_0$, featuring a circular profile [102]. Although it appears to be the optimized condition for producing symmetric structures, the longitudinal micromachining is usually avoided, once the waveguide length is limited by the working distance of the objective lens (ordinary close to 1 mm). In order to address this issue, the transversal writing has been used along with a cylindrical lens or slit that induces astigmatism in a proper direction to correct the asymmetry [102–104].

Even though femtosecond lasers are known for avoiding thermal effects in material processing, elevated repetition rates can make it considerable. Figure 11 illustrates the effect of repetition rate on the temperature during waveguide fabrication in alkali-free borosilicate. The irradiation condition (λ = 1045 nm, 375 fs, NA = 0.65) was used in the finite-difference thermal diffusion model, and a delta function in time was applied as the heat source, because the timescale for electron heating and electron-phonon coupling (<1 ps) is much shorter than the thermal diffusion time (>0.1 µs), according to the literature [100]. As one can see, for a repetition rate of 100 kHz, the temperature oscillates below and just above the working point of the glass (dashed line) each time a laser pulse achieves the network. For higher repetition rates, 0.5 and 1 MHz, there is a fast and significant increase of the temperature with the number of laser pulses, which keeps rising slowly with additional pulses. Thus, considering the time interval between consecutive pulses, the temperature behavior can be split into two regimes: (1) at low repetition rates, the thermal effects are repetitive and minimized because the heating follows the energy deposition by the laser pulses; and (2) at high repetition rates, there is not enough time for the lattice to cool down before the next pulse, resulting in heat accumulation and further increase of the temperature. Some researchers [105] found that the threshold between repetitive and cumulative effects is around 200 kHz for alkali-free borosilicate and low-alkali boroaluminosilicate glasses [100]. Conversely, Schaffer et al. obtained 1 MHz for a zinc-doped borosilicate glass, but they employed lower pulse energy and tighter focusing [106]. It is worth pointing out that there is a strong dependence on the experimental conditions and waveguide features. In general, the cumulative heating effect is favored by high pulse energy, high repetition rate and short wavelength that facilitate nonlinear interactions.

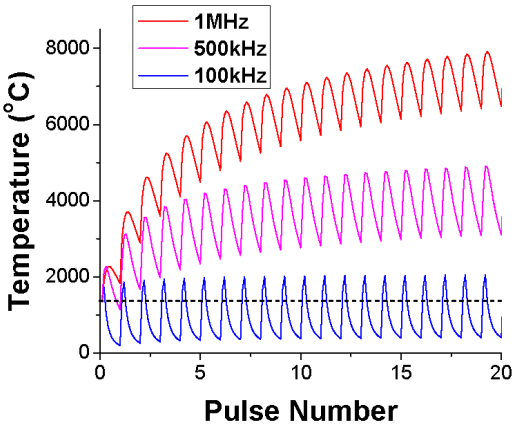

Figure 11. Finite-difference model of glass temperature versus laser exposure, at the position of 2 µm away from the center of the laser beam. Horizontal dashed line represents the 1225 °C working point of AF45 (alkali-free borosilicate) glass. Reprinted with permission from [105]. Copyright (2005), OSA.

3.5.2. Optical Waveguides in Glasses Containing Metal Nanoparticles

Optical waveguides containing metal nanoparticles can also be produced by taking advantage of the local heating caused by the cumulative effect from high repetition rate lasers, which makes it

possible not only to change the local density, but also to crystallize the glass matrix. Crystalline phases, from nanoparticles (NPs) to monocrystals, can be controlled inside the glass using a single-step laser processing. As mentioned before, the interaction between ultrashort laser pulses and the network leads to free electron generation. Cations in the glass matrix can react with these free electrons resulting in their reduction. Therefore, if the glass is doped with, for instance, Ag^{+}, Au^{3+}, Cu^{2+} ions, photoreduction reactions promote the formation of neutral atoms that further aggregate on account of the atomic mobility provided by the increase of temperature [35,36,107]. This procedure is summarized through Equations (1)–(3), which elucidate the formation of metallic silver nanoparticles by femtosecond-laser micromachining [36,108]. The same mechanism can be applied to other metals; nonetheless, one must consider the number of electrons involved in the photoreduction reaction.

$$Glass\ matrix \xrightarrow{h\nu} hole + e^{-} \quad (1)$$

$$Ag^{+} + e^{-} \rightarrow Ag^{0} \quad (2)$$

$$n\ Ag^{0} \xrightarrow{\Delta} n\ Ag_{n} \quad (3)$$

It is important to emphasize that the fs-laser is fundamental for the nucleation process, while the growth is achieved by some heating stage. Thus, if low repetition rate lasers are applied, annealing is required, configuring a two-step processing. Figure 12 clarifies the effects of high and low repetition rate lasers on the precipitation of copper and silver NPs in borosilicate glass [107,109]. The absorption spectra of pristine samples are represented by solid curve, while dotted and dashed curves display the absorbance after the irradiation using fs-lasers of 5 MHz (800 nm, 50 fs) and 1 kHz (775 nm, 150 fs) of repetition rate, respectively. Details about sample composition and experimental setup are described in Refs. [107,109].

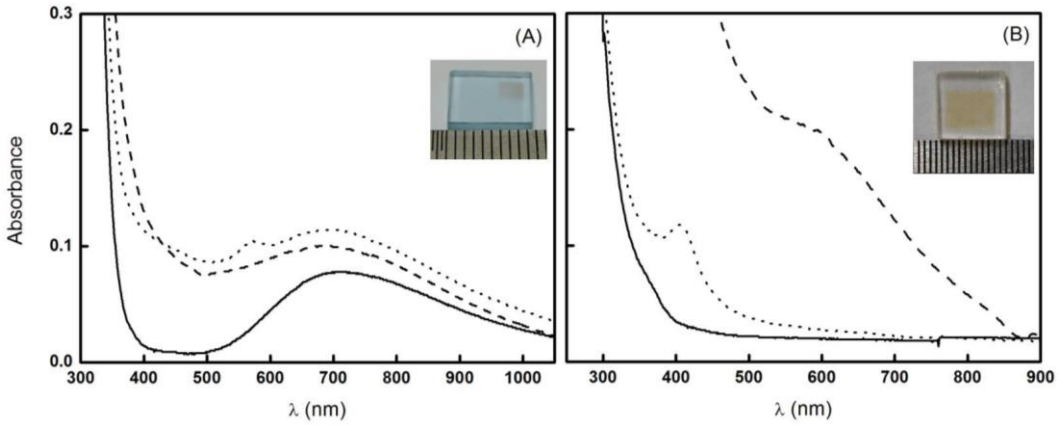

Figure 12. Absorption spectra of (**A**) copper-doped borosilicate glass and (**B**) silver-doped bariumborate glass. Solid lines represent the glasses as prepared, while dotted and dashed lines are the spectra after the irradiation with fs-lasers of 5 MHz and 1 kHz repetition rate respectively. Surface plasmon resonances of Cu^{0} and Ag^{0} nanoparticles are seen, respectively, at (**A**) 570 nm and (**B**) 410 nm. The insets show the sample picture containing the NPs. Reprinted with permission from [107,109]. Copyright (2012), OSA (for figure (**A**)) and Copyright (2013), Elsevier (for figure (**B**)).

Copper-doped sample originally presents a wide absorption band from 550–1000 nm due to the presence of Cu^{2+} ions, as seen in Figure 12a [107]. After receiving a dose of 1.5×10^{6} pulses/spot, corresponding to a fluence of 1.6 MJ/cm^{2} (5MHz laser), the surface plasmon resonance associated with Cu^{0} NPs is seen at 570 nm (dotted curve), assuring the nucleation and growth of the nanoparticles using a single laser scan. In fact, the observation of the plasmon band in the absorption spectrum is a practical way to check if the precipitation of metallic nanoparticles has occurred. On the other hand,

when the same sample was irradiated with 1 kHz repetition rate laser (delivering 30 pulses/spot, in which each spot experiences a fluence of 0.17 MJ/cm^2), instead of the plasmon band, an increase of the absorbance is observed. This increase for wavelengths shorter than 700 nm (dashed spectrum in Figure 12a) is related to electronic states created by the multiphoton absorption and ionization. They represent color center formations as well as photoreduction reactions, which lead to a preferential light absorption. Particularly, Cu^0 atoms cause a broad absorption band around 450 nm, indicating that the irradiation with 1 kHz laser induced the nucleation but not the growth of copper nanocrystals. The diffusion and aggregation of Cu^0 species was further achieved by a heat treatment at 600 °C for 1 h. Then, surface plasmon resonance was observed only in the irradiated region, resulting in an absorption spectrum quite similar to the one described for the case in which the irradiation was performed with high repetition rate.

Silver nanoparticles were produced and controlled three-dimensionally by direct laser writing in the same way [109]. The influence of low and high repetition rate lasers is shown in Figure 12b and can be explained following the previous example of copper NPs. In summary, Ag^0 nanoparticles readily precipitate when thermal effects associated with high repetition rates are presented, whereas lower repetition rates resulted in nucleation centers that subsequently grew on account of an additional annealing (400 °C for 1 h). In this case, the plasmon band of silver NPs is located at 410 nm, and effects caused by kHz laser pulses in a wide wavelength range, centered at 600 nm, are illustrated by dotted and dashed spectra of Figure 12b, respectively. A detailed study about the ionic species and clusters of silver induced by femtosecond laser was recently reported in the literature [110].

The interest in metallic nanoparticles in glass is based on the enhancement of optical properties provided by the surface plasmon resonance [111,112]. Therefore, the control of nanoparticle precipitation in very confined regions by fs-laser micromachining might be an important advance towards the development of metamaterials for all-optical devices. The growth of metallic NPs in the core of femtosecond-laser micromachined waveguides was recently demonstrated [36], according to the optical microscopy images in Figure 13. It has been discussed that the formation of Ag NPs, along with the waveguide fabrication, helps to improve the refractive index change, since an increase of 4.6% (or $\Delta n = 0.07$) has been reported due to the presence of silver NPs in silicate glasses [113].

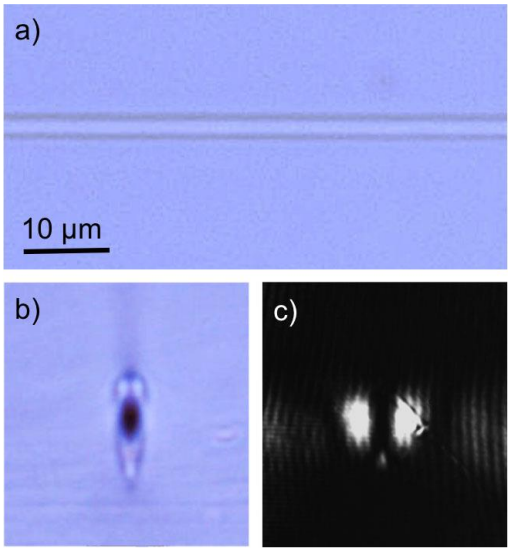

Figure 13. Optical microscopy images of the waveguide fabricated by fs-laser direct writing micromachining in silver-doped tungsten lead-pyrophosphate glass. Figures (**a**,**b**) show the top and end views respectively, while (**c**) displays the near-field output profile of the light guided at 632.8 nm. The scale bar for (**b**,**c**) is the same of (**a**). Reprinted with permission from [36]. Copyright (2014), AIP Publishing LLC.

Not only nanoparticles, but also nonlinear optical crystals have been grown by fs-laser writing in glasses. For instance, phase transition and growth of β-BaB_2O_4 (BBO), which is a frequency-conversion crystal, was demonstrated in glass [114]. Similarly, single crystal of lanthanum borogermanate ($LaBGeO_5$) with waveguide capability was also demonstrated [115]. Because of the lack of grain boundaries, this crystalline waveguide in glass displayed a good performance, yielding loss of 2.64 dB/cm at 1530 nm. While metallic nanoparticles in amorphous waveguides are important for the third-order optical nonlinearities, the crystalline phases enable the second-order properties. Also, laser-induced controlled crystallization has enabled the growth of phases not obtained by standard heat treatment, as in the case of euhedral crystal of $3PbO{\cdot}H_2O$ octahedrons, improving the architecture of microcrystals on glass surface [116]. Thus, fs-laser writing is a versatile and powerful tool for the development of photonic integrated circuits, configuring an important single-step processing of glassy materials.

Aiming the expansion of mid-infrared technologies, recent studies have focused on the fabrication of 3D waveguides in chalcogenide glasses, which combine the wide transparency over Mid-IR with higher optical nonlinearities, making them promising for supercontinuum generation, and light sources for mid-IR [117]. Because chalcogenide glass can present both negative and/or positive index change, different fs-laser writing methods have been proposed, as the helical trajectory which provides a negative cladding and positive waveguide core [118], or the hexagonal lattice, composed by several individual cores, allowing the tailoring of the refractive index contrast [119]. However, not only bulk chalcogenide glasses have been exploited for waveguides devoted to mid-IR region, but also chalcogenide thin films, in which bidimensional curved waveguides have been performed by fs-laser micromachining. These materials demonstrated significant spectral broadening [120], thereby assuring their potential for nonlinear optics and new infrared technologies.

3.6. Gold Ablation for Designing Microelectrodes

Fs-laser processing can also be used to fabricate interdigitated electrodes (IDEs) in metals for analytical chemical sensors, such as electronic tongues (e-tongue) [121–124] with high definition and accuracy. An interesting study on laser-induced heating, melting and ablation of metals, specifically aluminum, with a fundamental approach, has been recently published in Ref. [125]. In respect to IDEs, Manzolli et al. [126] reported the use of fs-laser-induced ablation for such a purpose. For that, glass substrate hosting a deposited bilayer film of chromium and gold with a thickness of 5 nm and 100 nm, respectively, were used as samples to be micromachined by a Ti:sapphire laser oscillator that emitted 50 fs pulses with energy up to 100 nJ at a repetition rate of 5.2 MHz. The samples were mounted in a motorized xy stage computer-controlled and positioned at the focus of a microscope objective, and parameters such as scanning velocity, objective numerical aperture and pulse energy were optimized. Analysis from optical and scanning electron microscopy showed that the coating material removal was uniform, accurate and continuous during the ablation process. Optimal experimental parameters included scanning velocity of 20 μm/s and pulse energy of 70 nJ focused by an objective of ×40 (NA = 0.65), which yielded 3.2 μm-wide fingers separated by a gap distance of 7.4 μm, according to scanning electron microscopy (SEM) images shown in Figure 14. Micromachining using higher pulse energies showed less control of the features fabricated, since with approximately 200 ns of pulse separation the heat accumulation became relevant. Novel techniques have also been developed in order to achieve higher resolution and control in nanowire fabrication. For example, Wang et al. added a spatial light modulator in the micromachining setup to overcome the diffraction limit and produce gold wires at nanoscale [127].

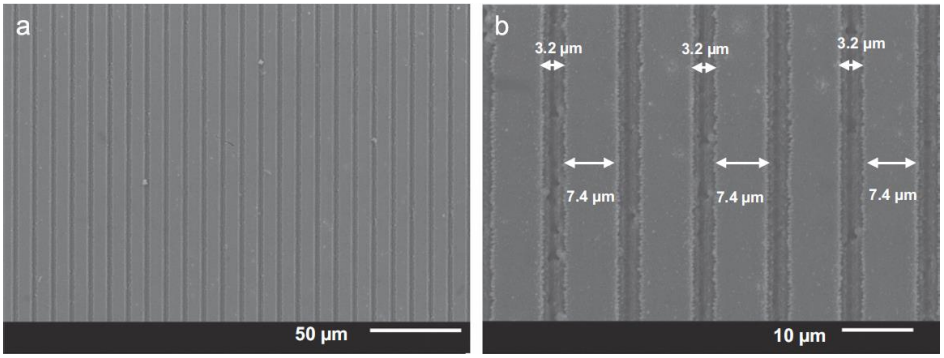

Figure 14. SEM images of interdigitated gold electrode fingers microfabricated using femtosecond-laser pulses. An overview image (**a**) and finger details (**b**) with distance measurements are shown in the figure. Reprinted with permission from [126]. Copyright (2015), Elsevier.

The comparison between the laser-ablated and conventional photolithography IDEs was evaluated using electrical impedance spectroscopy [128]. The IDE microfabricated via laser ablation showed better results, displaying lower resistance and higher capacitance. In addition, producing IDE via fs-laser processing is useful, since it is a reproducible, maskless and a single-step technique that is usually faster and versatile than traditional photolithography [129,130].

3.7. Micromachining Silicon Surfaces

Femtosecond-laser microstructuring can also be applied to microstructure silicon surfaces aiming at photovoltaic applications. The self-assembled conical structures formed at silicon surface after fs-pulse irradiation presents a significant increase in absorption and a decrease in reflectance in the visible and infrared spectra [131]. Such characteristics are addressed to a chemical composition change and an efficient light-trapping phenomenon due to the induced surface morphology. Thus, silicon-based devices, such as photodetectors and solar cells, are directly improved by the new optical properties achieved in microstructured silicon [132,133]. As of yet, solar cell devices fabricated using laser-textured silicon with efficiency as high as approximately 18% have been developed [134,135].

Silicon also presents an amorphous phase that has interesting applications in technology and opto-electronic devices. For instance, Almeida et al. [136] reported structural modification caused by femtosecond pulse irradiation on hydrogenated amorphous silicon (*a*-Si:H) films. Samples of *a*-Si:H films, with a thickness of 532 nm, were deposited over glass substrate by low-frequency glow discharge technique and further microstructured using a Ti:sapphire-amplified laser which delivered 150 fs pulses centered at 775 nm at 1 kHz repetition rate. A pair of galvanometric mirrors was used to scan the laser beam at the sample surface with a constant speed of 5 mm/s, while it was focused by a lens with focal distance of $f = 20$ cm yielding a 20 µm spot. At these conditions, two pulses were irradiated per area. The microstructuring of *a*-Si:H thin films led to surface texturing observed on scanning electron microscopy (SEM) images and visual color change resulted from a light-trapping phenomenon previously seen in crystalline silicon [137,138]. Raman spectra from crystalline silicon presented a sharp peak at 520.6 cm^{-1}, while *a*-Si:H films showed a broadband centered at 479 cm^{-1} before laser irradiation. Both spectra were used as reference to analyze the Raman signal from areas irradiated with different fluences, ranging from 1.8 to 6.2 MJ/m^2. As fluence increased, a small peak near 520 cm^{-1} was observed, indicating a laser-induced crystallization [139]. The crystallization phenomenon was later investigated by Belik et al. regarding its dependence on the fs-pulse central wavelength, where better results were achieved for pulses centered within 740–760 nm [140]. From such irradiated areas, atomic force microscopy (AFM) images revealed the formation of nanoscale spikes that increased in size for higher fluence until the point at which aggregation (globules) dominated the surface topography. With the aid of dedicated software [141], spikes were accurately identified by applying the Voronoi diagram,

generating height and radii histograms. *a*-Si:H films, which were not micromachined, presented a Gaussian distribution in their height histogram centered at 22 nm. For laser irradiation with fluence low enough to prevent spike aggregation, two overlapping Gaussian distributions were observed in its height histogram, one being the reminiscent distribution from the original sample and the other centered at 15 nm. The results indicate that laser-induced spikes are formed with smaller average height than original surface irregularities. For a higher fluence condition, a broader distribution centered at 40 nm agreed with the aggregation scenario, where structures with a higher and wider range of height are found. Radii histograms for non-irradiated films and a sample irradiated with low regime fluence (without inducing aggregation) presented the same characteristics of a Gaussian distribution centered at about 45 nm radius. This suggests that, at the early stage, laser-induced spikes are formed in domains already existing on the original sample surface and mainly change their height. Similar to the height histogram, radii distribution for the aggregated spikes is wider and centered at a higher value of radius.

4. Summary

In summary, femtosecond-laser micro/nanostructuring of materials has been proven to be a powerful tool for fabricating a variety of technological devices, from optical waveguides to surfaces with designed properties. This approach has enabled the modification of a wide range of materials at the surface and in the bulk with micro/nanometric resolution, with or without minimal undesirable features, such as debris and a heat-affected zone surrounding the focal volume. The several possible applications already demonstrated—and, in fact, currently being used in new technologies including role drilling [142], fabrication of microfluidic channels [143–145], optical storage devices [24,27,146] and waveguides [2,147–149]—give strength to the popularization of this approach for material modification and fabrication, especially because it is a low-cost and versatile alternative to traditional methods.

Acknowledgments: The authors are grateful to Fundação de Amparo à Pesquisa do Estado de São Paulo (FAPESP—2011/12399-0 and 2014/16789-5), Conselho Nacional de Desenvolvimento Científico e Tecnológico (CNPq), Coordenação de Aperfeiçoamento de Pessoal de Nível Superior (CAPES), EMBRAPA and MCTI from Brazil for financial support.

Conflicts of Interest: The authors declare no conflict of interest.

References

1. Davis, K.M.; Miura, K.; Sugimoto, N.; Hirao, K. Writing waveguides in glass with a femtosecond laser. *Opt. Lett.* **1996**, *21*, 1729–1731. [CrossRef] [PubMed]
2. Sikorski, Y.; Said, A.A.; Bado, P.; Maynard, R.; Florea, C.; Winick, K.A. Optical waveguide amplifier in Nd-doped glass written with near-IR femtosecond laser pulses. *Electron. Lett.* **2000**, *36*, 226–227. [CrossRef]
3. Florea, C.; Winick, K.A. Fabrication and characterization of photonic devices directly written in glass using femtosecond laser pulses. *J. Lightwave Technol.* **2003**, *21*, 246–253. [CrossRef]
4. Chichkov, B.N.; Momma, C.; Nolte, S.; von Alvensleben, F.; Tunnermann, A. Femtosecond, picosecond and nanosecond laser ablation of solids. *Appl. Phys. A Mater. Sci. Process.* **1996**, *63*, 109–115. [CrossRef]
5. Anisimov, S.I.; Kapeliov, B.L.; Perelman, T.L. Electron-emission from surface of metals induced by ultrashort laser pulses. *Zhurnal Eksperimentalnoi Teoreticheskoi Fiziki* **1974**, *66*, 776–781.
6. Nolte, S.; Momma, C.; Jacobs, H.; Tunnermann, A.; Chichkov, B.N.; Wellegehausen, B.; Welling, H. Ablation of metals by ultrashort laser pulses. *J. Opt. Soc. Am. B Opt. Phys.* **1997**, *14*, 2716–2722. [CrossRef]
7. Momma, C.; Nolte, S.; Chichkov, B.N.; von Alvensleben, F.; Tunnermann, A. Precise laser ablation with ultrashort pulses. *Appl. Surf. Sci.* **1997**, *109*, 15–19. [CrossRef]
8. Keldysh, L.V. Ionization in field of a strong electromagnetic wave. *Sov. Phys. JETP-Ussr* **1965**, *20*, 1307.
9. Schaffer, C.B.; Brodeur, A.; Mazur, E. Laser-induced breakdown and damage in bulk transparent materials induced by tightly focused femtosecond laser pulses. *Meas. Sci. Technol.* **2001**, *12*, 1784–1794. [CrossRef]
10. Stuart, B.C.; Feit, M.D.; Herman, S.; Rubenchik, A.M.; Shore, B.W.; Perry, M.D. Nanosecond-to-femtosecond laser-induced breakdown in dielectrics. *Phys. Rev. B* **1996**, *53*, 1749–1761. [CrossRef]

11. Zayarny, D.A.; Ionin, A.A.; Kudryashov, S.I.; Saraeva, I.N.; Startseva, E.D.; Khmelnitskii, R.A. Nonlinear absorption mechanisms during femtosecond laser surface ablation of silica glass. *JETP Lett.* **2016**, *103*, 309–312. [CrossRef]
12. Gamaly, E.G.; Juodkazis, S.; Nishimura, K.; Misawa, H.; Luther-Davies, B. Laser-matter interaction in the bulk of a transparent solid: Confined microexplosion and void formation. *Phys. Rev. B* **2006**, *73*, 214101. [CrossRef]
13. Bulgakova, N.M.; Bulgakov, A.V. Pulsed laser ablation of solids: Transition from normal vaporization to phase explosion. *Appl. Phys. A Mater. Sci. Process.* **2001**, *73*, 199–208. [CrossRef]
14. Nolte, S.; Will, M.; Burghoff, J.; Tuennermann, A. Femtosecond waveguide writing: A new avenue to three-dimensional integrated optics. *Appl. Phys. A Mater. Sci. Process.* **2003**, *77*, 109–111. [CrossRef]
15. Sun, H.B.; Xu, Y.; Juodkazis, S.; Sun, K.; Watanabe, M.; Matsuo, S.; Misawa, H.; Nishii, J. Arbitrary-lattice photonic crystals created by multiphoton microfabrication. *Opt. Lett.* **2001**, *26*, 325–327. [CrossRef] [PubMed]
16. Li, R.Z.; Peng, R.; Kihm, K.D.; Bai, S.; Bridges, D.; Tumuluri, U.; Wu, Z.; Zhang, T.; Compagnini, G.; Feng, Z.; et al. High-rate in-plane micro-supercapacitors scribed onto photo paper using in situ femtolaser-reduced graphene oxide/Au nanoparticle microelectrodes. *Energy Environ. Sci.* **2016**, *9*, 1458–1467. [CrossRef]
17. Zheng, C.; Hu, A.M.; Kihm, K.D.; Ma, Q.; Li, R.Z.; Chen, T.; Duley, W.W. Femtosecond Laser Fabrication of Cavity Microball Lens (CMBL) inside a PMMA substrate for super-wide angle imaging. *Small* **2015**, *11*, 3007–3016. [CrossRef] [PubMed]
18. Cheng, C.; Wang, S.T.; Wu, J.N.; Yu, Y.C.; Li, R.Z.; Eda, S.; Chen, J.G.; Feng, G.Y.; Lawrie, B.; Hu, A.M. Bisphenol A Sensors on Polyimide Fabricated by Laser Direct Writing for Onsite River Water Monitoring at Attomolar Concentration. *ACS Appl. Mater. Interfaces* **2016**, *8*, 17784–17792. [CrossRef] [PubMed]
19. Miura, K.; Qiu, J.R.; Inouye, H.; Mitsuyu, T.; Hirao, K. Photowritten optical waveguides in various glasses with ultrashort pulse laser. *Appl. Phys. Lett.* **1997**, *71*, 3329–3331. [CrossRef]
20. Chan, J.W.; Huser, T.; Risbud, S.; Krol, D.M. Structural changes in fused silica after exposure to focused femtosecond laser pulses. *Opt. Lett.* **2001**, *26*, 1726–1728. [CrossRef] [PubMed]
21. Chan, J.W.; Huser, T.R.; Risbud, S.H.; Krol, D.M. Modification of the fused silica glass network associated with waveguide fabrication using femtosecond laser pulses. *Appl. Phys. A Mater. Sci. Process.* **2003**, *76*, 367–372. [CrossRef]
22. Chan, J.W.; Huser, T.R.; Risbud, S.H.; Hayden, J.S.; Krol, D.M. Waveguide fabrication in phosphate glasses using femtosecond laser pulses. *Appl. Phys. Lett.* **2003**, *82*, 2371–2373. [CrossRef]
23. Burakov, I.M.; Bulgakova, N.M.; Stoian, R.; Mermillod-Blondin, A.; Audouard, E.; Rosenfeld, A.; Husakou, A.; Hertel, I.V. Spatial distribution of refractive index variations induced in bulk fused silica by single ultrashort and short laser pulses. *J. Appl. Phys.* **2007**, *101*. [CrossRef]
24. Glezer, E.N.; Milosavljevic, M.; Huang, L.; Finlay, R.J.; Her, T.H.; Callan, J.P.; Mazur, E. Three-dimensional optical storage inside transparent materials. *Opt. Lett.* **1996**, *21*, 2023–2025. [CrossRef] [PubMed]
25. Glezer, E.N.; Mazur, E. Ultrafast-laser driven micro-explosions in transparent materials. *Appl. Phys. Lett.* **1997**, *71*, 882–884. [CrossRef]
26. Schaffer, C.B.; Jamison, A.O.; Mazur, E. Morphology of femtosecond laser-induced structural changes in bulk transparent materials. *Appl. Phys. Lett.* **2004**, *84*, 1441–1443. [CrossRef]
27. Qiu, J.R.; Miura, K.; Hirao, K. Three-dimensional optical memory using glasses as a recording medium through a multi-photon absorption process. *Jpn. J. Appl. Phys. Part 1* **1998**, *37*, 2263–2266. [CrossRef]
28. Gorelik, T.; Will, M.; Nolte, S.; Tuennermann, A.; Glatzel, U. Transmission electron microscopy studies of femtosecond laser induced modifications in quartz. *Appl. Phys. A Mater. Sci. Process.* **2003**, *76*, 309–311. [CrossRef]
29. Itoh, K.; Watanabe, W.; Nolte, S.; Schaffer, C.B. Ultrafast processes for bulk modification of transparent materials. *MRS Bull.* **2006**, *31*, 620–625. [CrossRef]
30. Watanabe, W.; Li, Y.; Itoh, K. INVITED Ultrafast laser micro-processing of transparent material. *Opt. Laser Technol.* **2016**, *78*, 52–61. [CrossRef]
31. Tan, D.Z.; Sharafudeen, K.N.; Yue, Y.Z.; Qiu, J.R. Femtosecond laser induced phenomena in transparent solid materials: Fundamentals and applications. *Prog. Mater. Sci.* **2016**, *76*, 154–228. [CrossRef]
32. Nolte, S.; Chichkov, B.N.; Welling, H.; Shani, Y.; Lieberman, K.; Terkel, H. Nanostructuring with spatially localized femtosecond laser pulses. *Opt. Lett.* **1999**, *24*, 914–916. [CrossRef] [PubMed]

33. Schaffer, C.B.; Brodeur, A.; Garcia, J.F.; Mazur, E. Micromachining bulk glass by use of femtosecond laser pulses with nanojoule energy. *Opt. Lett.* **2001**, *26*, 93–95. [CrossRef] [PubMed]
34. Wolfe, D.B.; Ashcom, J.B.; Hwang, J.C.; Schaffer, C.B.; Mazur, E.; Whitesides, G.M. Customization of poly(dimethylsiloxane) stamps by micromachining using a femtosecond-pulsed laser. *Adv. Mater.* **2003**, *15*, 62–65. [CrossRef]
35. Qiu, J.R.; Jiang, X.W.; Zhu, C.S.; Shirai, M.; Si, J.; Jiang, N.; Hirao, K. Manipulation of gold nanoparticles inside transparent materials. *Angew. Chem. Int. Ed.* **2004**, *43*, 2230–2234. [CrossRef] [PubMed]
36. Almeida, J.M.P.; Ferreira, P.H.D.; Manzani, D.; Napoli, M.; Ribeiro, S.J.L.; Mendonca, C.R. Metallic nanoparticles grown in the core of femtosecond laser micromachined waveguides. *J. Appl. Phys.* **2014**, *115*. [CrossRef]
37. Mendonca, C.R.; Cerami, L.R.; Shih, T.; Tilghman, R.W.; Baldacchini, T.; Mazur, E. Femtosecond laser waveguide micromachining of PMMA films with azoaromatic chromophores. *Opt. Express* **2008**, *16*, 200–206. [CrossRef] [PubMed]
38. Liu, X.; Du, D.; Mourou, G. Laser ablation and micromachining with ultrashort laser pulses. *IEEE J. Quantum Electron.* **1997**, *33*, 1706–1716. [CrossRef]
39. Gattass, R.R.; Mazur, E. Femtosecond laser micromachining in transparent materials. *Nat. Photonics* **2008**, *2*, 219–225. [CrossRef]
40. Almeida, J.M.P.; De Boni, L.; Hernandes, A.C.; Mendonca, C.R. Third-order nonlinear spectra and optical limiting of lead oxifluoroborate glasses. *Opt. Express* **2011**, *19*, 17220–17225. [CrossRef] [PubMed]
41. Jenness, N.J.; Wu, Y.Q.; Clark, R.L. Fabrication of three-dimensional electrospun microstructures using phase modulated femtosecond laser pulses. *Mater. Lett.* **2012**, *66*, 360–363. [CrossRef]
42. Silvennoinen, M.; Kaakkunen, J.; Paivasaari, K.; Vahimaa, P. Parallel femtosecond laser ablation with individually controlled intensity. *Opt. Express* **2014**, *22*, 2603–2608. [CrossRef] [PubMed]
43. Torres-Peiro, S.; Gonzalez-Ausejo, J.; Mendoza-Yero, O.; Minguez-Vega, G.; Andres, P.; Lancis, J. Parallel laser micromachining based on diffractive optical elements with dispersion compensated femtosecond pulses. *Opt. Express* **2013**, *21*, 31830–31836. [CrossRef] [PubMed]
44. Lasagni, A.; Yuan, D.J.; Shao, P.; Das, S. Fabrication of periodic microstructures in pentaerythritol triacrylate through femtosecond laser interference two-photon. polymerization. *Adv. Eng. Mater.* **2009**, *11*, 595–599. [CrossRef]
45. Kondo, T.; Matsuo, S.; Juodkazis, S.; Misawa, H. Femtosecond laser interference technique with diffractive beam splitter for fabrication of three-dimensional photonic crystals. *Appl. Phys. Lett.* **2001**, *79*, 725–727. [CrossRef]
46. Kondo, T.; Matsuo, S.; Juodkazis, S.; Mizeikis, V.; Misawa, H. Multiphoton fabrication of periodic structures by multibeam interference of femtosecond pulses. *Appl. Phys. Lett.* **2003**, *82*, 2758–2760. [CrossRef]
47. Sun, H.B.; Kawata, S. Two-photon photopolymerization and 3D lithographic microfabrication. In *NMR—3D Analysis—Photopolymerization*; Springer-Verlag Berlim: Berlin, Germany, 2004; pp. 169–273.
48. Hell, S.W.; Wichmann, J. Breaking the diffraction resolution limit by stimulated-emission—Stimulated-emission-depletion fluorescence microscopy. *Opt. Lett.* **1994**, *19*, 780–782. [CrossRef] [PubMed]
49. Elmeranta, M.; Vicidomini, G.; Duocastella, M.; Diaspro, A.; de Miguel, G. Characterization of nanostructures fabricated with two-beam DLW lithography using STED microscopy. *Opt. Mater. Express* **2016**, *6*, 3169–3179. [CrossRef]
50. Fischer, J.; Wegener, M. Three-dimensional direct laser writing inspired by stimulated-emission-depletion microscopy Invited. *Opt. Mater. Express* **2011**, *1*, 614–624. [CrossRef]
51. Ferreira, P.H.D.; Stefanutti, R.; Pavinatto, F.J.; Mendonca, C.R. Femtosecond laser fabrication of waveguides in DR13-doped PMMA. *Opt. Commun.* **2014**, *318*, 53–56. [CrossRef]
52. Patzold, W.M.; Reinhardt, C.; Demircan, A.; Morgner, U. Cascaded-focus laser writing of low-loss waveguides in polymers. *Opt. Lett.* **2016**, *41*, 1269–1272. [CrossRef] [PubMed]
53. Kelb, C.; Patzold, W.M.; Morgner, U.; Rahlves, M.; Reithmeier, E.; Roth, B. Characterization of femtosecond laser written gratings in PMMA using a phase-retrieval approach. *Opt. Mater. Express* **2016**, *6*, 3202–3209. [CrossRef]
54. Bajpai, M.; Srivastava, R.; Kamalasanan, M.N.; Tiwari, R.S.; Chand, S. Charge transport and microstructure in PFO:MEH-PPV polymer blend thin films. *Synth. Met.* **2010**, *160*, 1740–1744. [CrossRef]

55. Si, J.H.; Qiu, J.R.; Zhai, J.F.; Shen, Y.Q.; Hirao, K. Photoinduced permanent gratings inside bulk azodye-doped polymers by the coherent field of a femtosecond laser. *Appl. Phys. Lett.* **2002**, *80*, 359–361. [CrossRef]
56. Estevam-Alves, R.; Ferreira, P.H.D.; Almeida, G.F.B.; Sousa, W.S.; Mendonca, C.R. Microfabrication of electroluminescent polymer for devices construction. *Appl. Surf. Sci.* **2014**, *314*, 633–637. [CrossRef]
57. Oliveira, S.L.; Correa, D.S.; De Boni, L.; Misoguti, L.; Zilio, S.C.; Mendonca, C.R. Two-photon absorption cross-section spectrum of a pi-conjugated polymer obtained using the white-light continuum Z-scan technique. *Appl. Phys. Lett.* **2006**, *88*. [CrossRef]
58. Ferreira, P.H.D.; Silva, D.L.; Misoguti, L.; Mendonca, C.R. MEH-PPV photobleaching control by femtosecond pulse shaping. *Phys. Status Solidi A Appl. Mater. Sci.* **2009**, *206*, 126–130. [CrossRef]
59. Otuka, A.J.G.; Almeida, J.M.P.; Tribuzi, V.; Cardoso, M.R.; Hernandes, A.C.; Correa, D.S.; Mendonca, C.R. Femtosecond Lasers for Processing Glassy and Polymeric Materials. *Mater. Res.-Ibero-Am. J. Mater.* **2014**, *17*, 352–358. [CrossRef]
60. Correa, D.S.; De Boni, L.; Otuka, A.J.G.; Tribuzi, V.; Mendonca, C.R. *Two-Photon Polymerization Fabrication of Doped Microstructures, in Polymerization*; Gomes, A.D.S., Ed.; Intech: Rijeka, Croatia, 2012; pp. 333–356.
61. Shukla, S.; Vidal, X.; Furlani, E.P.; Swihart, M.T.; Kim, K.T.; Yoon, Y.K.; Urbas, A.; Prasad, P.N. Subwavelength Direct Laser Patterning of Conductive Gold Nanostructures by Simultaneous Photopolymerization and Photoreduction. *ACS Nano* **2010**, *5*, 1947–1957. [CrossRef] [PubMed]
62. Kuo, W.S.; Lien, C.H.; Cho, K.C.; Chang, C.Y.; Lin, C.Y.; Huang, L.L.H.; Campagnola, P.J.; Dong, C.Y.; Chen, S.J. Multiphoton fabrication of freeform polymer microstructures with gold nanorods. *Opt. Express* **2010**, *18*, 27550–27559. [CrossRef] [PubMed]
63. Maruo, S.; Fourkas, J.T. Recent progress in multiphoton microfabrication. *Laser Photonics Rev.* **2008**, *2*, 100–111. [CrossRef]
64. Haske, W.; Chen, V.W.; Hales, J.M.; Dong, W.T.; Barlow, S.; Marder, S.R.; Perry, J.W. 65 nm feature sizes using visible wavelength 3-D multiphoton lithography. *Opt. Express* **2007**, *15*, 3426–3436. [CrossRef] [PubMed]
65. Fonseca, R.D.; Correa, D.S.; Paris, E.C.; Tribuzi, V.; Dev, A.; Voss, T.; Aoki, P.H.B.; Constantino, C.J.L.; Mendonca, C.R. Fabrication of Zinc Oxide Nanowires/Polymer Composites by Two-Photon. Polymerization. *J. Polym. Sci. Part. B Polym. Phys.* **2014**, *52*, 333–337. [CrossRef]
66. De Miguel, G.; Vicidomini, G.; Duocastella, M.; Diaspro, A. Selective fluorescence functionalization of dye-doped polymerized structures fabricated by direct laser writing (DLW) lithography. *Nanoscale* **2015**, *7*, 20164–20170. [CrossRef] [PubMed]
67. Furstner, R.; Barthlott, W.; Neinhuis, C.; Walzel, P. Wetting and self-cleaning properties of artificial superhydrophobic surfaces. *Langmuir* **2005**, *21*, 956–961. [CrossRef] [PubMed]
68. Wang, S.D.; Lin, B.J.; Hsieh, C.C.; Lin, C.C. Application of superhydrophobic sol gel on canvas. *Appl. Surf. Sci.* **2014**, *307*, 101–108. [CrossRef]
69. Zhu, J.; Hsu, C.-M.; Yu, Z.; Fan, S.; Cui, Y. Nanodome Solar Cells with Efficient Light Management and Self-Cleaning. *Nano Lett.* **2010**, *10*, 1979–1984. [CrossRef] [PubMed]
70. Cardoso, M.R.; Tribuzi, V.; Balogh, D.T.; Misoguti, L.; Mendonca, C.R. Laser microstructuring of azopolymers via surface relief gratings: Controlling hydrophobicity. *J. Optoelectron. Adv. Mater.* **2010**, *12*, 745–748.
71. Jiang, Z.L.; Fang, S.Y.; Wang, C.S.; Wang, H.P.; Ji, C.C. Durable polyorganosiloxane superhydrophobic films with a hierarchical structure by sol-gel and heat treatment method. *Appl. Surf. Sci.* **2016**, *390*, 993–1001. [CrossRef]
72. Guan, W.-S.; Huang, H.-X.; Chen, A.-F. Tuning 3D topography on biomimetic surface for efficient self-cleaning and microfluidic manipulation. *J. Micromech. Microeng.* **2015**, *25*, 35001–35009. [CrossRef]
73. Jin, K.J.; Cremaldi, J.C.; Erickson, J.S.; Tian, Y.; Israelachvili, J.N.; Pesika, N.S. Biomimetic Bidirectional Switchable Adhesive Inspired by the Gecko. *Adv. Funct. Mater.* **2014**, *24*, 574–579. [CrossRef]
74. Baldacchini, T.; Carey, J.E.; Zhou, M.; Mazur, E. Superhydrophobic surfaces prepared by microstructuring of silicon using a femtosecond laser. *Langmuir* **2006**, *22*, 4917–4919. [CrossRef] [PubMed]
75. Blossey, R. Self-cleaning surfaces—Virtual realities. *Nat. Mater.* **2003**, *2*, 301–306. [CrossRef] [PubMed]
76. Neinhuis, C.; Barthlott, W. Characterization and distribution of water-repellent, self-cleaning plant surfaces. *Ann. Bot.* **1997**, *79*, 667–677. [CrossRef]
77. Tuteja, A.; Choi, W.; Ma, M.L.; Mabry, J.M.; Mazzella, S.A.; Rutledge, G.C.; McKinley, G.H.; Cohen, R.E. Designing superoleophobic surfaces. *Science* **2007**, *318*, 1618–1622. [CrossRef] [PubMed]

78. Yan, Y.Y.; Gao, N.; Barthlott, W. Mimicking natural superhydrophobic surfaces and grasping the wetting process: A review on recent progress in preparing superhydrophobic surfaces. *Adv. Colloid Interface Sci.* **2011**, *169*, 80–105. [CrossRef] [PubMed]
79. Sun, T.; Feng, L.; Gao, X.; Jiang, L. Bioinspired surfaces with special wettability. *Accounts Chem. Res.* **2006**, *39*, 487. [CrossRef]
80. Chen, F.; Zhang, D.; Yang, Q.; Yong, J.; Du, G.; Si, J.; Yun, F.; Hou, X. Bioinspired Wetting Surface via Laser Microfabrication. *ACS Appl. Mater. Interfaces* **2013**, *5*, 6777–6792. [CrossRef] [PubMed]
81. Oner, D.; McCarthy, T.J. Ultrahydrophobic surfaces. Effects of topography length scales on wettability. *Langmuir* **2000**, *16*, 7777–7782. [CrossRef]
82. Wu, W.; Zhu, Q.; Qing, F.; Han, C.C. Water Repellency on a Fluorine-Containing Polyurethane Surface: Toward Understanding the Surface Self-Cleaning Effect. *Langmuir* **2009**, *25*, 17–20. [CrossRef] [PubMed]
83. Barberoglou, M.; Zorba, V.; Stratakis, E.; Spanakis, E.; Tzanetakis, P.; Anastasiadis, S.H.; Fotakis, C. Bio-inspired water repellent surfaces produced by ultrafast laser structuring of silicon. *Appl. Surf. Sci.* **2009**, *255*, 5425–5429. [CrossRef]
84. Otten, A.; Herminghaus, S. How plants keep dry: A physicist's point of view. *Langmuir* **2004**, *20*, 2405–2408. [CrossRef] [PubMed]
85. Vogelaar, L.; Lammertink, R.G.H.; Wessling, M. Superhydrophobic surfaces having two-fold adjustable roughness prepared in a single step. *Langmuir* **2006**, *22*, 3125–3130. [CrossRef] [PubMed]
86. Patankar, N.A. Mimicking the lotus effect: Influence of double roughness structures and slender pillars. *Langmuir* **2004**, *20*, 8209–8213. [CrossRef] [PubMed]
87. Jin, M.H.; Feng, X.J.; Xi, J.M.; Zhai, J.; Cho, K.W.; Feng, L.; Jiang, L. Super-hydrophobic PDMS surface with ultra-low adhesive force. *Macromol. Rapid Commun.* **2005**, *26*, 1805–1809. [CrossRef]
88. Cortese, B.; D'Amone, S.; Manca, M.; Viola, I.; Cingolani, R.; Gigli, G. Superhydrophobicity due to the hierarchical scale roughness of PDMS surfaces. *Langmuir* **2008**, *24*, 2712–2718. [CrossRef] [PubMed]
89. Feng, L.; Li, S.H.; Li, Y.S.; Li, H.J.; Zhang, L.J.; Zhai, J.; Song, Y.L.; Liu, B.Q.; Jiang, L.; Zhu, D.B. Super-hydrophobic surfaces: From natural to artificial. *Adv. Mater.* **2002**, *14*, 1857–1860. [CrossRef]
90. Yang, Y.-L.; Hsu, C.-C.; Chang, T.-L.; Kuo, L.-S.; Chen, P.-H. Study on wetting properties of periodical nanopatterns by a combinative technique of photolithography and laser interference lithography. *Appl. Surf. Sci.* **2010**, *256*, 3683–3687. [CrossRef]
91. Wu, B.; Zhou, M.; Li, J.; Ye, X.; Li, G.; Cai, L. Superhydrophobic surfaces fabricated by microstructuring of stainless steel using a femtosecond laser. *Appl. Surf. Sci.* **2009**, *256*, 61–66. [CrossRef]
92. Cardoso, M.R.; Martins, R.J.; Dev, A.; Voss, T.; Mendonca, C.R. Highly hydrophobic hierarchical nanomicro roughness polymer surface created by stamping and laser micromachining. *J. Appl. Polym. Sci.* **2015**, *132*, 4. [CrossRef]
93. Bonse, J.; Rosenfeld, A.; Krueger, J. Femtosecond laser-induced periodic surface structures: Recent approaches to explain their sub-wavelength periodicities. In Proceedings of the Lat 2010: International Conference on Lasers, Applications, and Technologies, Kazan, Russia, 7 February 2011.
94. Cassie, A.B.D.; Baxter, S. Wettability of porous surfaces. *Trans. Faraday Soc.* **1944**, *40*, 0546–0550. [CrossRef]
95. Zorba, V.; Persano, L.; Pisignano, D.; Athanassiou, A.; Stratakis, E.; Cingolani, R.; Tzanetakis, P.; Fotakis, C. Making silicon hydrophobic: Wettability control by two-lengthscale simultaneous patterning with femtosecond laser irradiation. *Nanotechnology* **2006**, *17*, 3234–3238. [CrossRef]
96. Kietzig, A.-M.; Hatzikiriakos, S.G.; Englezos, P. Patterned Superhydrophobic Metallic Surfaces. *Langmuir* **2009**, *25*, 4821–4827. [CrossRef] [PubMed]
97. Li, B.J.; Li, H.; Huang, L.J.; Ren, N.F.; Kong, X. Femtosecond pulsed laser textured titanium surfaces with stable superhydrophilicity and superhydrophobicity. *Appl. Surf. Sci.* **2016**, *389*, 585–593. [CrossRef]
98. Tien, A.C.; Backus, S.; Kapteyn, H.; Murnane, M.; Mourou, G. Short-pulse laser damage in transparent materials as a function of pulse duration. *Phys. Rev. Lett.* **1999**, *82*, 3883–3886. [CrossRef]
99. Almeida, J.M.P.; Fonseca, R.D.; De Boni, L.; Diniz, A.R.S.; Hernandes, A.C.; Ferreira, P.H.D.; Mendonca, C.R. Waveguides and nonlinear index of refraction of borate glass doped with transition metals. *Opt. Mater.* **2015**, *42*, 522–525. [CrossRef]
100. Will, M.; Nolte, S.; Chichkov, B.N.; Tunnermann, A. Optical properties of waveguides fabricated in fused silica by femtosecond laser pulses. *Appl. Opt.* **2002**, *41*, 4360–4364. [CrossRef] [PubMed]

101. Veiko, V.P.; Kudryashov, S.I.; Sergeev, M.M.; Zakoldaev, R.A.; Danilov, P.A.; Ionin, A.A.; Antropova, T.V.; Anfimova, I.N. Femtosecond laser-induced stress-free ultra-densification inside porous glass. *Laser Phys. Lett.* **2016**, *13*, 055901. [CrossRef]
102. Osellame, R.; Taccheo, S.; Marangoni, M.; Ramponi, R.; Laporta, P.; Polli, D.; De Silvestri, S.; Cerullo, G. Femtosecond writing of active optical waveguides with astigmatically shaped beams. *J. Opt. Soc. Am. B-Opt. Phys.* **2003**, *20*, 1559–1567. [CrossRef]
103. Ams, M.; Marshall, G.D.; Spence, D.J.; Withford, M.J. Slit beam shaping method for femtosecond laser direct-write fabrication of symmetric waveguides in bulk glasses. *Opt. Express* **2005**, *13*, 5676–5681. [CrossRef] [PubMed]
104. Cheng, Y.; Sugioka, K.; Midorikawa, K.; Masuda, M.; Toyoda, K.; Kawachi, M.; Shihoyama, K. Control. of the cross-sectional shape of a hollow microchannel embedded in photostructurable glass by use of a femtosecond laser. *Opt. Lett.* **2003**, *28*, 55–57. [CrossRef] [PubMed]
105. Eaton, S.; Zhang, H.; Herman, P.; Yoshino, F.; Shah, L.; Bovatsek, J.; Arai, A. Heat accumulation effects in femtosecond laser-written waveguides with variable repetition rate. *Opt. Express* **2005**, *13*, 4708–4716. [CrossRef] [PubMed]
106. Schaffer, C.B.; Garcia, J.F.; Mazur, E. Bulk heating of transparent materials using a high-repetition-rate femtosecond laser. *Appl. Phys. A Mater. Sci. Process.* **2003**, *76*, 351–354. [CrossRef]
107. Almeida, J.M.P.; De Boni, L.; Avansi, W.; Ribeiro, C.; Longo, E.; Hernandes, A.C.; Mendonca, C.R. Generation of copper nanoparticles induced by fs-laser irradiation in borosilicate glass. *Opt. Express* **2012**, *20*, 15106–15113. [CrossRef] [PubMed]
108. Coelho, J.M.P.; Silva, C.; Ruivo, A.; Matos, A.P. Infrared Nanosecond Laser Radiation in the Creation of Gold and Copper Nanoparticles. *Mater. Sci. Forum* **2013**, *730*, 915–919.
109. Almeida, J.M.P.; Tribuzi, V.; Fonseca, R.D.; Otuka, A.J.G.; Ferreira, P.H.D.; Mastelaro, V.R.; Brajato, P.; Hernandes, A.C.; Dev, A.; Voss, T.; et al. Femtosecond laser processing of glassy and polymeric matrices containing metals and semiconductor nanostructures. *Opt. Mater.* **2013**, *35*, 2643–2648. [CrossRef]
110. Marquestaut, N.; Petit, Y.; Royon, A.; Mounaix, P.; Cardinal, T.; Canioni, L. Three-dimensional silver nanoparticle formation using femtosecond laser irradiation in phosphate glasses: Analogy with photography. *Adv. Funct. Mater.* **2014**, *24*, 5824–5832. [CrossRef]
111. Sekhar, H.; Kiran, P.P.; Rao, D.N. Structural, linear and enhanced third-order nonlinear optical properties of Bi12SiO20 nanocrystals. *Mater. Chem. Phys.* **2011**, *130*, 113–120. [CrossRef]
112. Smolorz, S.; Kang, I.; Wise, F.; Aitken, B.G.; Borrelli, N.F. Studies of optical non-linearities of chalcogenide and heavy-metal oxide glasses. *J. Non-Cryst. Solids* **1999**, *256*, 310–317. [CrossRef]
113. Dai, Y.; Yu, G.; He, M.; Ma, H.; Yan, X.; Ma, G. High repetition rate femtosecond laser irradiation-induced elements redistribution in Ag-doped glass. *Appl. Phys. B-Lasers Opt.* **2011**, *103*, 663–667. [CrossRef]
114. Miura, K.; Qiu, J.R.; Mitsuyu, T.; Hirao, K. Space-selective growth of frequency-conversion crystals in glasses with ultrashort infrared laser pulses. *Opt. Lett.* **2000**, *25*, 408–410. [CrossRef] [PubMed]
115. Stone, A.; Jain, H.; Dierolf, V.; Sakakura, M.; Shimotsuma, Y.; Miura, K.; Hirao, K.; Lapointe, J.; Kashyap, R. Direct laser-writing of ferroelectric single-crystal waveguide architectures in glass for 3D integrated optics. *Sci. Rep.* **2015**, *5*, 10391. [CrossRef] [PubMed]
116. Almeida, J.M.P.; Almeida, G.F.B.; Hernandes, A.C.; Mendonca, C.R. Architecture of lead oxide microcrystals in glass: A laser and etching based method. *CrystEngComm* **2016**, *18*, 5959–5964. [CrossRef]
117. Demetriou, G.; Berube, J.P.; Vallee, R.; Messaddeq, Y.; Petersen, C.R.; Jain, D.; Bang, O.; Craig, C.; Hewak, D.W.; Kar, A.K. Refractive index and dispersion control of ultrafast laser inscribed waveguides in gallium lanthanum sulphide for near and mid-infrared applications. *Opt. Express* **2016**, *24*, 6350–6358. [CrossRef] [PubMed]
118. Caulier, O.; Masselin, P.; Bychkov, E.; Le Coq, D. INVITED Tailoring the morphology of photowritten buried waveguides by helical trajectory in As2S3 glass. *Opt. Laser Technol.* **2016**, *78*, 56–61. [CrossRef]
119. Masselin, P.; Bychkov, E.; Le Coq, D. Direct laser writing of a low-loss waveguide with independent control over the transverse dimension and the refractive index contrast between the core and the cladding. *Opt. Lett.* **2016**, *41*, 3507–3510. [CrossRef] [PubMed]
120. Almeida, J.M.P.; Barbano, E.C.; Arnold, C.B.; Misoguti, L.; Mendonça, C.R. Nonlinear optical waveguides in As2S3-Ag2S chalcogenide glass thin films. *Opt. Mater. Express* **2017**, *7*, 93–99. [CrossRef]

121. Riul, A.; de Sousa, H.C.; Malmegrim, R.R.; dos Santos, D.S.; Carvalho, A.; Fonseca, F.J.; Oliveira, O.N.; Mattoso, L.H.C. Wine classification by taste sensors made from ultra-thin films and using neural networks. *Sens. Actuators B Chem.* **2004**, *98*, 77–82. [CrossRef]
122. Legin, A.; Rudnitskaya, A.; Vlasov, Y.; Di Natale, C.; Davide, F.; D'Amico, A. Tasting of beverages using an electronic tongue. *Sens. Actuators B Chem.* **1997**, *44*, 291–296. [CrossRef]
123. Bueno, L.; Paixao, T.R.L.C. A copper interdigitated electrode and chemometrical tools used for the discrimination of the adulteration of ethanol fuel with water. *Talanta* **2011**, *87*, 210–215. [CrossRef] [PubMed]
124. Kirsanov, D.; Legin, E.; Zagrebin, A.; Ignatieva, N.; Rybakin, V.; Legin, A. Mimicking Daphnia magna bioassay performance by an electronic tongue for urban water quality control. *Anal. Chim. Acta* **2014**, *824*, 64–70. [CrossRef] [PubMed]
125. Kudryashov, S.I.; Ionin, A.A. Multi-scale fluence-dependent dynamics of front-side femtosecond laser heating, melting and ablation of thin supported aluminum film. *Int. J. Heat Mass Transf.* **2016**, *99*, 383–390. [CrossRef]
126. Manzoli, A.; de Almeida, G.F.B.; Filho, J.A.; Mattoso, L.H.C.; Riul, A., Jr.; Mendonca, C.R.; Correa, D.S. Femtosecond laser ablation of gold interdigitated electrodes for electronic tongues. *Opt. Laser Technol.* **2015**, *69*, 148–153. [CrossRef]
127. Wang, A.D.; Jiang, L.; Li, X.W.; Liu, Y.; Dong, X.Z.; Qu, L.T.; Duan, X.M.; Lu, Y.F. Mask-free patterning of high.-conductivity metal. nanowires in open air by spatially modulated femtosecond laser pulses. *Adv. Mater.* **2015**, *27*, 6238–6243. [CrossRef] [PubMed]
128. Riul, A., Jr.; Dantas, C.A.R.; Miyazaki, C.M.; Oliveira, O.N., Jr. Recent advances in electronic tongues. *Analyst* **2010**, *135*, 2481–2495. [CrossRef] [PubMed]
129. Martin, J.I.; Nogues, J.; Liu, K.; Vicent, J.L.; Schuller, I.K. Ordered magnetic nanostructures: Fabrication and properties. *J. Magn. Magn. Mater.* **2003**, *256*, 449–501. [CrossRef]
130. Mijatovic, D.; Eijkel, J.C.T.; van den Berg, A. Technologies for nanofluidic systems: Top-down vs. bottom-up—A review. *Lab. Chip* **2005**, *5*, 492–500. [CrossRef] [PubMed]
131. Wu, C.; Crouch, C.H.; Zhao, L.; Carey, J.E.; Younkin, R.; Levinson, J.A.; Mazur, E.; Farrell, R.M.; Gothoskar, P.; Karger, A. Near-unity below-band-gap absorption by microstructured silicon. *Appl. Phys. Lett.* **2001**, *78*, 1850–1852. [CrossRef]
132. Carey, J.E.; Crouch, C.H.; Shen, M.Y.; Mazur, E. Visible and near-infrared responsivity of femtosecond-laser microstructured silicon photodiodes. *Opt. Lett.* **2005**, *30*, 1773–1775. [CrossRef] [PubMed]
133. Huang, Z.H.; Carey, J.E.; Liu, M.G.; Guo, X.Y.; Mazur, E.; Campbell, J.C. Microstructured silicon photodetector. *Appl. Phys. Lett.* **2006**, *89*. [CrossRef]
134. Iyengar, V.V.; Nayak, B.K.; Gupta, M.C. Optical properties of silicon light trapping structures for photovoltaics. *Sol. Energy Mater. Sol. Cells* **2010**, *94*, 2251–2257. [CrossRef]
135. Nayak, B.K.; Iyengar, V.V.; Gupta, M.C. Efficient light trapping in silicon solar cells by ultrafast-laser-induced self-assembled micro/nano structures. *Prog. Photovolt.* **2011**, *19*, 631–639. [CrossRef]
136. Almeida, G.F.B.; Cardoso, M.R.; Aoki, P.H.B.; Lima, J.J.D., Jr.; Costa, L.D.F.; Rodrigues, C.A.; Constantino, C.J.L.; Mendonca, C.R. Surface morphology and structural modification induced by femtosecond pulses in hydrogenated amorphous silicon films. *J. Nanosci. Nanotechnol.* **2015**, *15*, 2495–2500. [CrossRef] [PubMed]
137. Her, T.H.; Finlay, R.J.; Wu, C.; Mazur, E. Femtosecond laser-induced formation of spikes on silicon. *Appl. Phys. A Mater. Sci. Process.* **2000**, *70*, 383–385. [CrossRef]
138. Crouch, C.H.; Carey, J.E.; Warrender, J.M.; Aziz, M.J.; Mazur, E.; Genin, F.Y. Comparison of structure and properties of femtosecond and nanosecond laser-structured silicon. *Appl. Phys. Lett.* **2004**, *84*, 1850–1852. [CrossRef]
139. Korchagina, T.T.; Gutakovsky, A.K.; Fedina, L.I.; Neklyudova, M.A.; Volodin, V.A. Crystallization of amorphous Si nanoclusters in SiOx films using femtosecond laser pulse annealings. *J. Nanosci. Nanotechnol.* **2012**, *12*, 8694–8699. [CrossRef] [PubMed]
140. Belik, V.P.; Vasyutinskii, O.S.; Kukin, A.V.; Petrov, M.A.; Popov, R.S.; Terukov, E.I. Crystallization of amorphous hydrogenated silicon (a-Si:H) films under irradiation with femtosecond laser pulses. *Tech. Phys. Lett.* **2016**, *42*, 788–791. [CrossRef]

141. Costa, L.D.; Rodrigues, C.A.; de Souza, N.C.; Oliveira, O.N. Statistical characterization of morphological features of layer-by-layer polymer films by image analysis. *J. Nanosci. Nanotechnol.* **2003**, *3*, 257–261. [CrossRef]
142. Liu, X.B. Industrial applications of ultrahigh precision short-pulse laser processing. In Proceedings of Processing in Microelectronics and Photonics IV, San Jose, CA, USA, 22 January 2005.
143. Iga, Y.; Ishizuka, T.; Watanabe, W.; Itoh, K.; Li, Y.; Nishii, J. Characterization of micro-channels fabricated by in-water ablation of femtosecond laser pulses. *Jpn. J. Appl. Phys. Part 1* **2004**, *43*, 4207–4211. [CrossRef]
144. Hnatovsky, C.; Taylor, R.S.; Simova, E.; Bhardwaj, V.R.; Rayner, D.M.; Corkum, P.B. Polarization-selective etching in femtosecond laser-assisted microfluidic channel fabrication in fused silica. *Opt. Lett.* **2005**, *30*, 1867–1869. [CrossRef] [PubMed]
145. Ho, S.; Herman, P.R.; Aitchison, J.S. Single- and multi-scan femtosecond laser writing for selective chemical etching of cross section patternable glass micro-channels. *Appl. Phys. A Mater. Sci. Process.* **2012**, *106*, 5–13. [CrossRef]
146. Cheng, G.H.; Wang, Y.S.; Liu, Q.; Zhao, W.; Chen, G.F. Study of three-dimensional storage by parallel writing in PMMA with femtosecond laser pulses. *Acta Phys. Sin.* **2004**, *53*, 436–440.
147. Streltsov, A.M.; Borrelli, N.F. Fabrication and analysis of a directional coupler written in glass by nanojoule femtosecond laser pulses. *Opt. Lett.* **2001**, *26*, 42–43. [CrossRef] [PubMed]
148. Minoshima, K.; Kowalevicz, A.M.; Ippen, E.P.; Fujimoto, J.G. Fabrication of coupled mode photonic devices in glass by nonlinear femtosecond laser materials processing. *Opt. Express* **2002**, *10*, 645–652. [CrossRef] [PubMed]
149. Taccheo, S.; Della Valle, G.; Osellame, R.; Cerullo, G.; Chiodo, N.; Laporta, P.; Svelto, O.; Killi, A.; Morgner, U.; Lederer, M.; et al. Er: Yb-doped waveguide laser fabricated by femtosecond laser pulses. *Opt. Lett.* **2004**, *29*, 2626–2628. [CrossRef] [PubMed]